FEDERAL UNIVERSITY OF PERNAMBUCO
TECHNOLOGY AND GEOCIENCES CENTER
MECHANICAL ENGINEERING GRADUATE PROGRAM

PEDRO HENRIQUE MATTOS MELO

A MULTIPOINT FLUX APPROXIMATION FINITE VOLUME METHOD FOR THE NUMERICAL SIMULATION OF THE STOKES-BRINKMAN PROBLEM IN 2-D USING UNSTRUCTURED MESHES

Recife

2021

PEDRO HENRIQUE MATTOS MELO

A MULTIPOINT FLUX APPROXIMATION FINITE VOLUME METHOD FOR THE NUMERICAL SIMULATION OF THE STOKES-BRINKMAN PROBLEM IN 2-D USING UNSTRUCTURED MESHES

Thesis submitted to the faculty of the Mechanical Engineering Graduate Program of the Federal University of Pernambuco, as part of the requirements necessary to obtain a Master's degree in Mechanical Engineering.

Area of Concentration:: Energy

Surpervisor : Paulo Roberto Maciel Lyra, PhD.

Co-Surpervisor : Darlan Karlo Elisiário de Carvalho, PhD.

Recife

2021

Catalogação na fonte
Bibliotecária Margareth Malta, CRB-4 / 1198

M528m Melo, Pedro Henrique Mattos.
A multipoint flux approximation finite volume method for the numerical simulation of the stokes-brinkman problem in 2-D using unstructured meshes / Pedro Henrique Mattos Melo. - 2021.
78 folhas, il., gráfs., tabs.

Orientador: Prof. Dr. Paulo Roberto Maciel Lyra.
Coorientador: Prof. Dr. Darlan Karlo Elisiário de Carvalho.

Dissertação (Mestrado) – Universidade Federal de Pernambuco. CTG. Programa de Pós-Graduação em Engenharia Mecânica, 2021.
Inclui Referências e Apêndice.
Texto em inglês.

1. Engenharia mecânica. 2. Reservatórios carbonáticos. 3. Modelo de Stokes-Brinkman. 4. Método dos volumes finitos. 5. MPFA-H. 6. SIMPLEC. I. Lyra, Paulo Roberto Maciel (Orientador). II. Carvalho, Darlan Karlo Elisiário de (Coorientador). III. Título.

UFPE

621 CDD (22. ed.) BCTG/2021-80

PEDRO HENRIQUE MATTOS MELO

A MULTIPOINT FLUX APPROXIMATION FINITE VOLUME METHOD FOR THE NUMERICAL SIMULATION OF THE STOKES-BRINKMAN PROBLEM IN 2-D USING UNSTRUCTURED MESHES

Dissertação apresentada ao Programa de Pós-Graduação em Engenharia Mecânica do Departamento de Engenharia Mecânica, Centro de Tecnologia e Geociências da Universidade Federal de Pernambuco como parte dos requisitos parciais para obtenção do título de mestre em Engenharia Mecânica.

Aprovada em: 19/03/2021

BANCA EXAMINADORA

Prof. Dr. Paulo Roberto Maciel Lyra (Orientador)

Universidade Federal de Pernambuco

Prof. Dr. Darlan Karlo Elisiário de Carvalho (Coorientador)

Universidade Federal de Pernambuco

Prof. Dr. Maicon Ribeiro Corrêa (Examinador Externo)

Universidade Estadual de Campinas

Prof. Dr. Alessandro Romário Echevarria Antunes (Examinador Externo)

Universidade Federal de Pernambuco

Dedico este trabalho a minha mãe e a meus avós maternos, que sempre me incentivaram e me apoiaram em todos os momentos e decisões.

ACKNOWLEDGEMENTS

First and foremost, I would like to thank God and the Holy Mary, whose help and blessings made possible to finish this thesis.

I thank my maternal grandparents Mariano Pedro Mattos and Shirley Gomes de Mattos (in memoriam) whose support and guidance were essential to my formation.

I thank my mother, Flávia Mattos, that is my safe port, that help me no matter the circumstances and was essential to me, especially, at the final stage of this thesis.

I thank Professors Paulo Lyra and Darlan Karlo for the opportunity and guidance.

I thank all the colleagues of PADMEC for sharing their knowledge with me, especially Professor Fernando for our code and help during the final stages of this thesis.

I thank FACEPE, CAPES and CNPq for the financial support.

Em primeiro lugar, gostaria de agradecer a Deus e a Nossa Senhora, cuja ajuda e bençãos possibilitaram o término desta tese.

Agradeço a meus avós maternos Mariano Pedro Mattos e Shirley Gomes de Mattos (*in memoriam*) cujo suporte e orientação foram essenciais para minha formação.

Agradeço a minha mãe, Fávia Mattos, que é meu porto seguro, que me ajuda em qualquer circunstância e que foi essencial para mim, principalmente, nas fases finais desta dissertação.

Agradeço aos Professores Paulo Lyra e Darlan Karlo pela oportunidade e orientação.

Agradeço a todos os colegas do grupo PADMEC por compartilhar seus conhecimentos, em especial o Professor Fernando pelo nosso código e ajuda durante os estágios finais desta dissertação.

Agradeço à FACEPE, CAPES e CNPq pelo suporte financeiro.

"Talvez não tenha conseguido fazer o melhor, mas lutei para que o melhor fosse feito. Não sou o que deveria ser, mas Graças a Deus, não sou o que era antes."

(Marthin Luther King)

ABSTRACT

Fractures, vugs, cavities and caves can significantly alter the fluid flow on carbonate petroleum reservoirs, making the computational simulation even more challenging due to the existence of free flow (Stokes) and porous media flow (Darcy). Different strategies can be devised to handle this problem, including the triple porosity and single permeability, the triple porosity and triple permeability etc. A much more accurate modeling can be done by using the so-called Darcy-Stokes model. In this approach, the Darcy´s Law is used in the porous media domain and the Stokes equation is used in the free flow region. However, for carbonate petroleum reservoirs the use of this model is extremely complex due to the difficulties of accurately representing the geometrical intricacies of the naturally fractured media. An alternative approach is to use the Stokes-Brinkman (S-B) model. In this formulation, a single equation, is used to represent the fluid flow in both, the free flow region and in the porous media. This approach avoids the explicit modeling of the interface between the two domains, by transitioning between them automatically. In this context, in the present thesis, we have used the S-B model to represent the fluid flow in the entire reservoir rock. To solve the system of equations, we have used a cell-centered finite volume scheme based on harmonic points (MPFA-H) and the Rhie and Chow's interpolation to ensure the coupling between the variables. The MPFA-H is a robust method that can handle heterogeneous and anisotropic media on unstructured polygonal meshes. Finally, we have compared the SIMPLEC (Semi Implicit Method for Pressure Linked Equations Consistent) and the monolithic approaches to solve the system of equations. The proposed formulation presented good results, especially regarding the physical representation of the Stokes and Darcy models in the so-called free-flow and porous medium domains, respectively, demonstrating proximity to data available in the literature, considering the same flow conditions.

Keywords: Carbonate Reservoirs, Stokes-Brinkman Model, Finite Volume Method, MPFA-H, SIMPLEC.

RESUMO

Fraturas, *vugs* e cavernas podem alterar significativamente o escoamento de fluidos em reservatórios carbonáticos de petróleo, tornando a simulação computacional ainda mais desafiadora devido a existência de escoamento livre (Stokes) e escoamento em meios porosos (Darcy). Diferentes estratégias são utilizadas para superar este problema, icluindo modelos de tripla porosidade, tripla porosidade e tripla permeabilidade, etc. Uma modelagem muito mais acurada pode ser obtida com a utilização do chamado modelo Darcy-Stokes. Neste caso, a Lei de Darcy é utilizada na região de meio poroso e a equção de Stokes é utilizada na região de escoamento livre. Porém, em reservatórios carbonáticos de petróleo a utilização de tal modelo pode ser extremamente complexo devido as dificuldades de representar de forma acurada a geometria de meios natuuralmente fraturados. Uma abordagem alternativa é a utilização do modelo de Stokes-Brinkman (S-B). Nesta formulação, uma única equação, é usada para representar o escoamento do fluido tanto na região de meio poroso quanto de escoamento livre. Esta abordagem evita a necessidade de modelar explicitamente a interface entre os dois domínios, fazendo esta transição de maneira automática. Neste contexto, no presente trabalho, o modelo de S-B foi utilizado para representar o escoamento do fluido em todo reservatório. Para resolver o sistema de equações foi utilizado uma formulação de volumes finitos centrada na célula baseado em pontos harmônicos (MPFA-H) e o método de interpolação de Rhie-Chow foi utilizado para garantir o acoplamento entre as variáveis. O MPFA-H é um método robusto, capaz de lidar com meios heterogêneos e anisotrópicos em malhas poligonais não estruturadas. Por fim, comparou-se os resultados da formulação segregada, SIMPLEC (*Semi Implicit Method for Pressure Linked Equations Consistent*) e a monolítica. A formulação proposta apresentou bons resultados, principalmente no que diz respeito a representação física dos modelos de Stokes e Darcy nos domínios ditos de fluxo livre e meio poroso, respectivamente, demonstrando proximidade com dados disponíveis na literatura, considerando as mesmas condições de escoamento.

Palavras-chaves: Reservatórios Carbonáticos, Modelo de Stokes-Brinkman, Método dos Volumes Finitos, MPFA-H, SIMPLEC.

LIST OF FIGURES

LIST OF TABLES

LIST OF ABBREVIATIONS AND ACRONYMS

2-D	Two Dimensions
3-D	Three Dimensions
CFD	Computational Fluid Dynamics
CV	Control Volume
FDM	Finite Difference Method
FEM	Finite Element Method
FVM	Finite Volume Method
MIM	Momentum Interpolation Method
MPFA	Multipoint Flux Approximmation Methods
MPFA-H	Multipoint Flux Approximmation based on Harmonic Points
PDE	Partial Differential Equation
SIMPLE	Semi Implicit Linked Equations
SIMPLEC	Semi Implicit Linked Equations Consistent

CONTENTS

1 INTRODUCTION

Carbonate Karstic reservoirs are commonly found around the world, such as in China (AHR et al., 2005), Middle East (DABBOUK et al., 2002), in the Brazilian Pre-Salt region (DOROBEK et al., 2012). Some estimates relates that 60% of the world's oil reserve lie in carbonate reservoirs (SPADINI et al., 2008).

A diagenetic processes that occurs on carbonate reservoirs on account of the chemical nature of the carbonate rocks, associated to the phenomena of tectonization and karstification, originate geological features such as vugs, small to medium size voids, and caves, large size voids, that can be interconnected or not involving multiple scales (BI et al., 2009; KROTKIEWSKI et al., 2011; HE et al., 2015).

The presence of these geological features on multiple scales, represents a challenge to numerical simulation of fluid flow in these reservoirs due the highly heterogeneous rock properties and the coexistence of two different flow regions, a Darcian flow region in the porous media and a free flow region in the vugs, cavities and caves, making the coupled approximate numerical modeling of the fluid flow in these reservoirs very challenging (CONCEIÇÃO et al., 2019). Different approaches are used to model the fluid flow on these reservoirs, two possible mathematical models for modeling the fluid flow in carbonate reservoirs are the continuum models and discontinuum models (YAO et al., 2010).

Triple-continuum models, due it simplicity, are the most popular continuum model (VELAZQUEZ et al., 2005; WU et al., 2007), in which three overlap continua, the rock matrix, the fractures and the karstic region, are all treated as a porous media with homogeneous and uniform properties (HALLACK; FILHO; COUTO, 2019). Another approach is to represent the three continua, the rock matrix, the fracture and the vugs, as an unique equivalent media by adopting a homogenization of the permeabilities and porosities of the domain. Although simple, particularly in terms of computational efforts, it is extremely demanding to approximate the equivalent properties properly. Furthermore, as a consequence of it, the continuum models can not account the coexistence of the porous and the free flow region.

Alternatively, the discontinuum model represents the discontinuities of the rock in a discretized form, in such manner that it may be a natural and interesting approach when dealing with media that presents such complex fluid flow pattern (GOLFIER; LASSEUX; QUINTARD, 2014). When using a double domain model, the most common approach is adopt the so-called

Darcy-Stokes model Arbogast and Lehr (2006), Yao et al. (2010), in which the porous media is modeled using the Darcy equation, in the matrix region, and, in the free flow regions, using the Stokes equation. By adopting these strategies, additional interface conditions must be used to guarantee the mass conservation and linear momentum conservation along the interface between the porous media region and free flow region (HE et al., 2015).

An alternative approach to model the fluid flow on highly heterogeneous carbonate reservoirs, using a discontinuum model, is to employ the Stokes-Brinkman's equation (BRINKMAN, 1949), in which a single equation is used to model the fluid flow in the porous media and free flow regions. Furthermore, by adopting this approach, there is no need of modeling, explicitly, interface conditions alongside the different flow regions (BI et al., 2009; LAPTEV, 2003; KROTKIEWSKI et al., 2011).

In literature, different strategies are used to simulate the fluid flow on carbonate reservoirs, using the Stokes-Brinkman's equation. For example, He et al. (2015) and Conceição et al. (2019) adopted a formulation based on Finite Difference Method (FDM) when dealing with structured meshes, Bi et al. (2009) applied the Finite Element Method (FEM) and a upscaling process to solve the Stokes-Brinkman's equation on unstructured meshes.

Multipoint Flux Approximation (MPFA) methods have been widely used in the last decades to discretize fluid flow problems in porous media that are modeled by the Darcy equation (AAVATSMARK et al., 1998a; AAVATSMARK et al., 1998b; AHMED et al., 2015; FRIIS; EDWARDS, 2011; CAVALCANTE et al., 2020; CONTRERAS; LYRA; de Carvalho, 2019; QUEIROZ et al., 2014; CONTRERAS et al., 2016) MPFA methods are robust and flexible to handle full permeability tensors and unstructured meshes. Recently, (ILIEV et al., 2014) has adapted the MPFA-O method to model the Stokes-Brinkman problem using structured quadrilateral meshes. In this context, and due the presence of the vugs and caves on karstic reservoirs, that have different properties when compared with the rock matrix (OLSON; LAUBACH; LANDER, 2007), and the need for a more precise geometric representation of the vugs, the Multipoint Flux Approximmation Methods (MPFA) method, arises as a numerical scheme capable of handling the characteristics of these reservoirs.

In this thesis, a full pressure suport MPFA-H originnaly proposed by Gao and Wu (2013), for the first time in literature, is extended to discretize the Stokes-Brinkman's equations to allow the simulation using nonhomogeneous, anisotropic permeablity tensors, using unstructured meshes.

1.1 MOTIVATION

A great deal of proven oil reserves lays on carbonate reservoirs. Due the karstification process, these reservoirs have a great deal of uncertainties in production forecasts, associated to geological models and the fluid flow pattern, notably in the regions where these process is prominent.

Another aspect is the lack of work in literature, particularly when dealing with anisotropic media and unstructured meshes. In that fashion, and bearing in mind the importance of the oil industry, the study of a unified model that can depict the fluid flow, and diminish the uncertainties of production, when dealing with carbonate reservoirs are the motivation of this work.

1.2 RESEARCH OBJECTIVES

Within this frame of reference, the general objectives of this thesis is the study and development of a finite volume scheme for the 2-D numerical simulation of a one-phase flow on heterogeneous and anisotropic carbonate petroleum reservoirs, using general polygonal meshes.

1.2.1 Specific Objectives

1. Develop a framework for the simulation of one-phase flow on heterogeneous and anisotropic carbonate reservoirs using a flux approximation consistent with unstructured grids.
2. Incorporate the MPFA-H to solve the Stokes-Brinkman equation.
3. Investigate the influence of the karstic structures on the pressure and velocity fields, considering a incompressible fluid flow.

1.3 THESIS ORGANIZATION

This thesis is constituted by 6 different chapters. In this first chapter a review of carbonate reservoirs and the issues regarding the simulation of one-phase flow on these reservoirs are addressed. The second chapter comprises the mathematical formulation used to derive the Partial Differential Equation (PDE) that described the flow on carbonate reservoirs. The third

chapter is dedicated to the numerical formulation, in which, we present the numerical scheme used to approximate the equations of the previous chapter. In the fourth chapter, we present a monolithic and a segregate solution for the Stokes-Brinkman equation, using SIMPLEC algorithm. In the fifth chapter the numerical results for a single-phase flow are presented. Ultimately, in the sixth chapter we present the conclusions and suggestions for further work.

2 MATHEMATICAL FORMULATION

In this chapter, a concise introduction of the laws and hypothesis used to derive the equations that govern the fluid flow on porous media and free flow regions are presented. First we describe the mass conservation PDE, that model the pressure distribution along the reservoir, and the linear momentum PDE that represents the phenomena. Furthermore, we will discuss three different formulation for the conservation of momentum equation:

1. Stokes Equation,
2. Darcy Equation, and
3. Stokes Brinkman Equation.

2.1 SIMPLIFYING HYPOTHESES

Due the complexity associated to the fluid flow on these reservoirs, it is essential the usage of physical-mathematical simplifications. In this fashion, we adopted in this work the following simplifying hypotheses:

1. The fluid flow is considered a single-phase flow,
2. The fluid is considered Newtonian,
3. The rock is considered incompressible and it is fully saturated with the fluid,
4. All chemical reactions, thermical effects and capillarity effects are neglected,
5. The effects of gravity are neglected.

2.2 MASS CONSERVATION EQUATION

Let us consider a medium that is fully saturated with a single-phase fluid. The mass conservation equation states that for a given volume V fully saturated and inclosed by a surface A, the variation of the mass inside this volume, at any time t, is equal to the net mass flow rate in the absence of source terms (HIRSCH, 2007; EWING, 1983; BEAR, 2013).

Considering the simplifying hypothesis, we can apply the mass conservation for all continuous domain as:

$$\Phi c_t \frac{\partial \rho}{\partial t} + \nabla(\rho \mathbf{u}) = q_m \tag{2.1}$$

where ρ is the fluid density, $\mathbf{u}$ is the fluid velocity vector, Φ is the porosity, c_t is the media compressibility and q_m is the source term.

Considering the fluid incompressible and homogeneous i.e. the fluid density does not change in time and space and without any source terms, we can simplify Equation 2.1 as:

$$\nabla \cdot \mathbf{u} = 0 \tag{2.2}$$

2.3 DARCY'S LAW

The Darcy's Law is based on the experiments of Henry Darcy on water flow through a bed sands (DARCY, 1856). Darcy's Law is valid when the scale of the problem is more considerable when compared with pore scale, in this fashion it is a volume average of the Navier-Stokes equation (EWING, 1983). Darcy's law states that for a single phase fluid, the fluid velocity is proportional to the pressure gradient, as described by the equation bellow:

$$\mathbf{u} = -\frac{\mathbf{K}}{\mu} \nabla p \tag{2.3}$$

where $\mathbf{K}$ is the rock permeability tensor, μ is the fluid viscosity and p is the pore average pressure distributed throughout the inside the reservoir (HALLACK; FILHO; COUTO, 2019).

In Equation 2.3, the rock absolute permeability tensor, $\mathbf{K}$, by adopting Cartesian coordinate system in a two dimensional space is given by:

$$\mathbf{K} = \begin{bmatrix} k_{xx} & k_{xy} \\ k_{yx} & k_{yy} \end{bmatrix} \tag{2.4}$$

The absolute permeability $\mathbf{K}$ is an intrinsic property of the rock and it denotes the capacity of the medium to permit the flow.

2.4 STOKES' EQUATION

Usually, the system of equations that represents the Navier-Stokes Equation are composed by the mass conservation equation, Equation 2.1, previously discussed and the conservation

of linear momentum equation (DREW; PASSMAN, 1999).

The linear momentum conservation equation is based on the Newton's Second Law i.e. the momentum net rate on any portion of fluid must be equal to the sum of all the forces acting on this same portion:

$$\frac{D(\rho \mathbf{u})}{Dt} = -\nabla \cdot \tau - \nabla p + \rho g + F \tag{2.5}$$

in which, τ is the shear stress tensor, g is the gravity and F is the summation of all external forces.

By assuming the hypotheses suggested by (STOKES, 1845; GLOVER, 1994) we can finally define de well known Navier-Stokes Equation:

$$\frac{D(\rho \mathbf{u})}{Dt} = \mu \nabla^2 \mathbf{u} - \nabla p + \rho g \tag{2.6}$$

in which the term $\mu \nabla^2 \mathbf{u}$ is known as diffusive viscosity term and $\frac{D(\rho \mathbf{u}}{Dt}$ represents the total acceleration, that is divided on an instantaneous acceleration (transient term) and a advective acceleration, moreover the term ρg depict the gravitational force influence.

When dealing with a fluid flow with a low Reynolds Number, $Re < 1$, the inertial forces can be neglected, once the effects of the viscous forces are predominant on the fluid flow (BATCHELOR, 2000). In that way, Equation 2.6 can be simplyfied as:

$$\mu \nabla^2 \mathbf{u} - \nabla p + \rho g = 0 \tag{2.7}$$

Equation 2.7 is known as Stokes Equation, that can be used to analyse the fluid flow in the karstic domain of the carbonate petroleum reservoirs, because the fluid flow in this geological formations has a low Re and the flow is considered a free flow (HE et al., 2015; CONCEIÇÃO et al., 2019)

2.5 STOKES-BRINKMAN EQUATION

Occasionally, it is possible to encounter in nature porous media with high values of porosity. In that fashion, the carbonate reservoirs can be included in this group due the presence of vugs and caves.

For media with these characteristics, the Darcy's Law, often, does not show a good agreement with experimental results, specially when dealing with high permeability media. With the intention of overcome these problem, Brinkman (BRINKMAN, 1949) studied the effects of viscous forces exerted for the fluid flow over a swarm of particles.

Brinkman proposed a model for the fluid flow in which a modification was made on the Darcy's Law, Equation 2.3, by adding the viscous term present on Stoke's Equation, Equation 2.7, in a empiracal form such that, in the stationary regime, is given by Equation 2.8

$$\nabla p = -\frac{\mu}{\mathbf{K}}\mathbf{u} + \mu^{'}\nabla^2\mathbf{u} \tag{2.8}$$

where $\mu^{'}$ is the fluid effective viscosity.

The fluid effective viscosity, also know as the Brinkman's effective viscosity, is widely discussed in literature (AURIAULT; BOUTIN; GEINDREAU, 2010; MARTYS; BENTZ; GARBOCZI, 1994; BRINKMAN, 1949). In this work, on the grounds that the effects of suspended particles are neglected, consider the dynamic and effective viscosity is a good approximation for the model (CARMAN, 1997).

For a typical carbonate reservoir, inside of which there are two types of fluid flow regions the Equation 2.8 reduces to Darcy Equation on the porous media domain, wherein the term $\mu\mathbf{K}^{-1}\mathbf{u}$ prevails over the term $\mu\nabla^2\mathbf{u}$ by orders of magnitude. On the other hand, in the free flow regions, in the free flow regions, inside the karstics structures, where the values of permeability are much bigger than in the porous media, ideally $\mathbf{K} \to \infty$, the term $\mu\nabla^2\mathbf{u}$ becomes predominant and Equation 2.8 tends to Stokes Equation (2.7) (KROTKIEWSKI et al., 2011; CONCEIÇÃO et al., 2019; HE et al., 2015)

2.6 INITIAL AND BOUNDARY CONDITIONS

To completely define the system of equations that governs the fluid flow, and make the mathematical model well-posed, a proper combination of initial and boundary conditions must be applied. A typical set of boundary conditions are (CONTRERAS et al., 2017; CARVALHO, 2005; CONCEIÇÃO et al., 2019):

$$\begin{aligned} p(\mathbf{x_D}, t) &= g_D \quad \text{in} \quad \Gamma_D \times T \\ \mathbf{u}\cdot\mathbf{n} &= g_N \quad \text{in} \quad \Gamma_N \times T \\ \mathbf{u}(\mathbf{x}, 0) &= \mathbf{u}^0 \quad \text{in} \quad \Omega \quad at \quad t = 0 \\ \mathbf{u}(\mathbf{x}, t) &= 0 \quad in \quad \Gamma_S \times T \end{aligned} \tag{2.9}$$

in which Γ_D and Γ_N represent the Neumman and Dirichlet boundaries conditions, respectively, Γ_S denotes the solid wall boundaries and T is the time interval of the analysis. The scalar g_D (prescribed pressure), g_N (prescribed flux) are applied defined at Γ_N and Γ_D respectively and Γ is the domain.

Figure 1 – Computational Domain Identifying the injection and production well, and the Neumman and Dirichlet boundaries

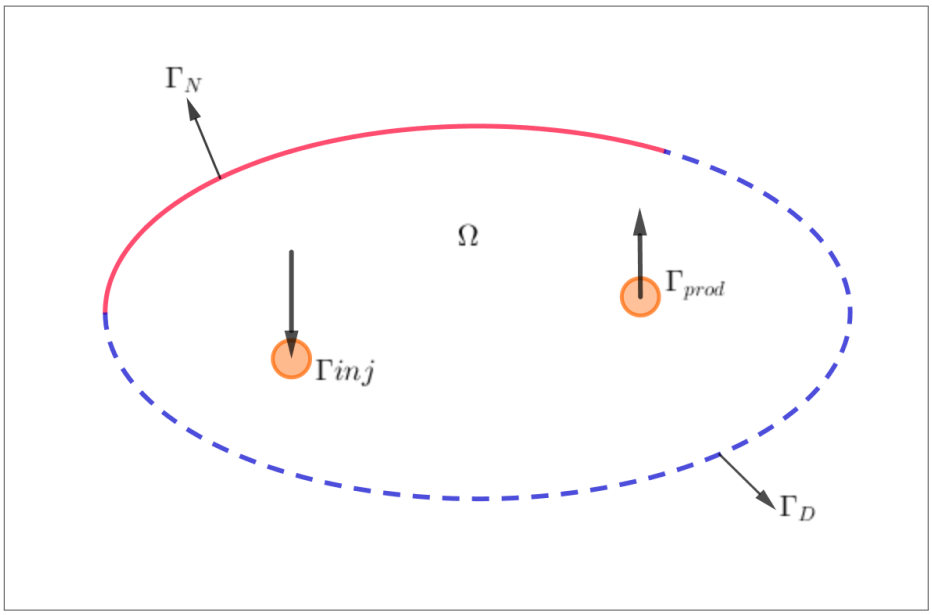

Source: Author.

The contour of the domain Ω, represented by $\partial\Omega$, can be considered as a disjunct union of the other countors:

$$\partial\Omega = \Gamma_S \cup \Gamma_D \cup \Gamma_D \cup \Gamma_{prod} \cup \Gamma_{inj} \tag{2.10}$$

in which, Γ_{prod} and Γ_{inj} represents the production and injection wells, respectively, as shown in Figure 1.

3 NUMERICAL FORMULATION

In this chapter, we present the numerical strategy used to numerically solve the PDEs presented in the last chapter. A large number of methods, were developed to do so, among them, the Finite Volume Method (FVM), that provides conservative solutions.

3.1 VARIABLE ARRANGEMENT

Due the weak coupling between the variables, pressure and velocity that exists in some equations, such as Navier-Stokes and Stokes-Brinkman equations, different grid arrangements were used to face this problem.

The staggered grid arrangement described by Patankar (2018) in which the values of pressures are stored at the centroid of the control volume and the components of velocities, namelly u and v, are stored at the cell faces (edge in 2-D). As a consequence, the problems related to the so called checker-board pressure fields, are solved, despite that by using a staggered grid arrangement it may became unmanageable in Three Dimensions (3-D) and even for curvilinear and circular grids, and, consequently for unstructured meshes (FERZIGER; PERIĆ; STREET, 2020; MARCHI; MALISKA, 1994).

An alternative variable arrangement is the cell-centered, in which all the variables are stored at the center of the control volume (CARVALHO, 2005; FERZIGER; PERIĆ; STREET, 2020). By doing that, and due to the weak couple of the variables it mandatory to use some strategy that ensure the coupling, but the computational implementation of the numerical method becomes simple even for 3-D cases (RHIE; CHOW, 1983; MAZUMDER, 2015).

In this work, we adopted a cell-centered finite volume scheme alongside a momentum interpolation method to ensure the coupling between the variables, that will be further explained in the next sections.

3.2 FINITE VOLUME DISCRETIZATION OF STOKES-BRINKMAN EQUATION

Initially, we should rewrite the Equation 2.8 considering a transient term regarding the velocity components. Thus, we can define a system of equations, Equation 3.1 , composed by the the mass conservation equation and the Stokes-Brinkman Equation in the transient

regime:

$$\begin{cases} \frac{\partial(\rho \mathbf{u})}{\partial t} + \mu \mathbf{K}^{-1}\mathbf{u} - \mu' \nabla^2 \mathbf{u} = -\nabla p \\ \nabla \mathbf{u} = 0 \end{cases} \tag{3.1}$$

Assuming that the computational domain is two-dimensional, the Equation 3.1 can be rewrite in terms of the cartesian velocity components u and v, that represents the velocities in the x and y direction, respectively.

$$\begin{cases} \frac{\partial(\rho u)}{\partial t} + \mu \mathbf{K}^{-1}u - \mu' \nabla^2 u = \frac{\partial p}{\partial x} \\ \frac{\partial(\rho v)}{\partial t} + \mu \mathbf{K}^{-1}v - \mu' \nabla^2 v = \frac{\partial p}{\partial y} \\ \frac{\partial u}{\partial x} + \frac{\partial v}{\partial y} = 0 \end{cases} \tag{3.2}$$

On the basis of the FVM, the approximate solution of Equation 3.1, the conservation of momentum equation and the divergence free velocity equation, is obtained by integrating it throughout the domain Ω, which leads to:

$$\int_\Omega \frac{\partial(\rho \mathbf{u})}{\partial t}\, d\Omega + \int_\Omega \mu \mathbf{K}^{-1}\mathbf{u}\, d\Omega - \int_\Omega \mu' \nabla^2 \mathbf{u}\, d\Omega = -\int_\Omega \nabla p\, d\Omega \tag{3.3}$$

$$\int_\Omega \nabla u\, d\Omega = 0 \tag{3.4}$$

Figure 2 – Discrete domain and general control volume $\Omega_{\hat{L}}$

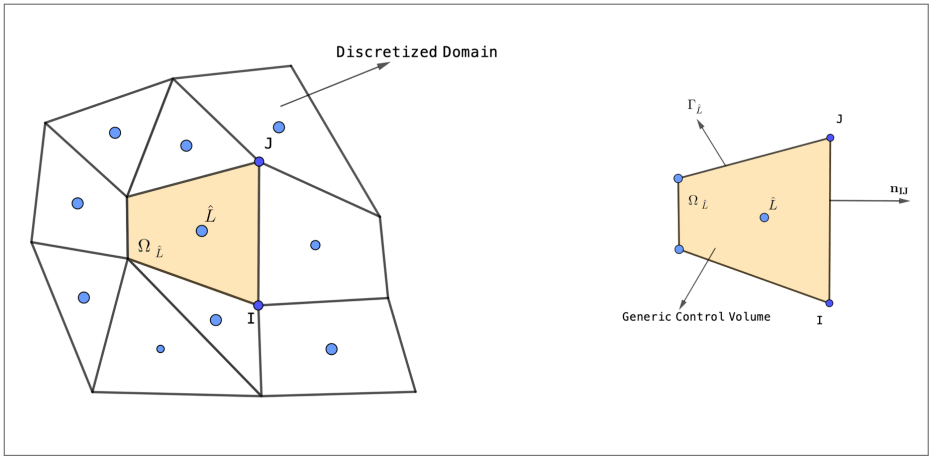

Source: Author.

In order to obtain a discrete form of Equation 3.3 and 3.4, the domain Ω is subdivided in a series of n_v Control Volume (CV) $\Omega_{\hat{L}}$, as shown on Figure 2. In that fashion, we can rewrite

Equation 3.3 and 3.4 as a sum of integrals over all the n_v CV:

$$\sum_{i=1}^{n_v} \int_{\Omega_{\hat{L}}} \frac{\partial(\rho \mathbf{u})}{\partial t} \, d\Omega_{\hat{L}} + \sum_{i=1}^{n_v} \int_{\Omega_{\hat{L}}} \mu \mathbf{K}^{-1} \mathbf{u} \, d\Omega_{\hat{L}} - \sum_{i=1}^{n_v} \int_{\Omega_{\hat{L}}} \mu^{'} \nabla^2 \mathbf{u} \, d\Omega_{\hat{L}} = - \sum_{i=1}^{n_v} \int_{\Omega_{\hat{L}}} \nabla p \, d\Omega_{\hat{L}} \quad (3.5)$$

$$\sum_{i=1}^{n_v} \int_{\Omega_{\hat{L}}} \nabla u \, d\Omega_{\hat{L}} = 0 \quad (3.6)$$

In the following subsections we will address all the terms separately. Initially, the momentum equation will be discretized using the MPFA-H, soon after the mass conservation equation will be discretized alongside a Momentum Interpolation Method (MIM) in order to guarantee the coupling between the variables.

3.2.1 Pressure Gradient

The pressure gradient, with respect to each control volume $\Omega_{\hat{L}}$, fourth term of Equation 3.5 is approximate by employing the Green-Gauss's divergence theorem, as:

$$- \sum_{i=1}^{n_v} \int_{\Omega_{\hat{L}}} \nabla p \, d\Omega_{\hat{L}} = - \sum_{IJ \in \Gamma_{\hat{L}}} \int_{IJ} p \mathbf{n}_{\Gamma_{IJ}} ds = - \sum_{IJ \in \Gamma_{\hat{L}}} p_{IJ} \, \|IJ\| \, \mathbf{n}_{IJ} \quad (3.7)$$

where $p_{IJ} = \frac{1}{\|IJ\|} \int_{IJ} p ds$ and $\mathbf{n}_{IJ}$ is the outward unit normal with respect to the face IJ and p_{IJ} stands for the pressure at the control surfaces in $\Omega_{\hat{L}}$, with $\|IJ\|$ referring to the area (length in 2-D) of the face $\|IJ\|$. In (ILIEV et al., 2014) the author adopted the cell face midpoint as interpolation point, however in the present work we have adopted the so-called harmonic interpolation points (CONTRERAS et al., 2017).

3.2.1.1 Interpolation Strategy Using Harmonic Points

The definition and derivation of harmonic points adopted in this paper, was firstly proposed by (AGELAS; EYMARD; HERBIN, 2009).

Consider two control volumes, $\hat{L}$ and $\hat{R}$, adjacent to a face IJ of the domain, with respective permeability tensors $\mathbf{K}_{\hat{\mathbf{L}}}$ and $\mathbf{K}_{\hat{\mathbf{R}}}$ and $x_{\hat{L}} \in \hat{L}$ and $x_{\hat{R}} \in \hat{R}$ the corresponding centroids of the control volumes, see Figure 5. With the purpose of obtaining a method with a small stencil, we need to find a point over the face IJ in which the solution is a combination, solely, of the pressures of the adjacent control volumes, $p_{\hat{L}}$ and $p_{\hat{R}}$. In that sense, we can write the

co-normal vectors $\mathbf{K}_{\hat{\mathbf{L}}}^{\top}$ and $\mathbf{K}_{\hat{\mathbf{R}}}^{\top}$ as follows:

$$\mathbf{K}_{\hat{\mathbf{L}}}^{\top}\mathbf{n_{IJ}} = a_{\hat{L}}(x_{\hat{L},i(IJ)} - x_{\hat{L}}) + b_{\hat{L}}(J - I) \tag{3.8}$$

and

$$\mathbf{K}_{\hat{\mathbf{R}}}^{\top}\mathbf{n_{IJ}} = a_{\hat{R}}(x_{\hat{R}} - x_{\hat{R},i(IJ)}) + b_{\hat{R}}(J - I) \tag{3.9}$$

For each face (edge in 2-D) of a control volume $\hat{L}$ it is always possible to define two auxiliary points, designated by $x_{\hat{L},i(IJ)}$ and $x_{\hat{L},j(IJ)}$, which are the harmonic points, in a way that the vectors $\overrightarrow{x_{\hat{L}}x_{\hat{L},i(IJ)}}$ and $\overrightarrow{x_{\hat{L}}x_{\hat{L},j(IJ)}}$ are not collinear, as it can be seen in Figure 3.

Figure 3 – Representation of the physical and geometric parameters for the MPFA-H method.

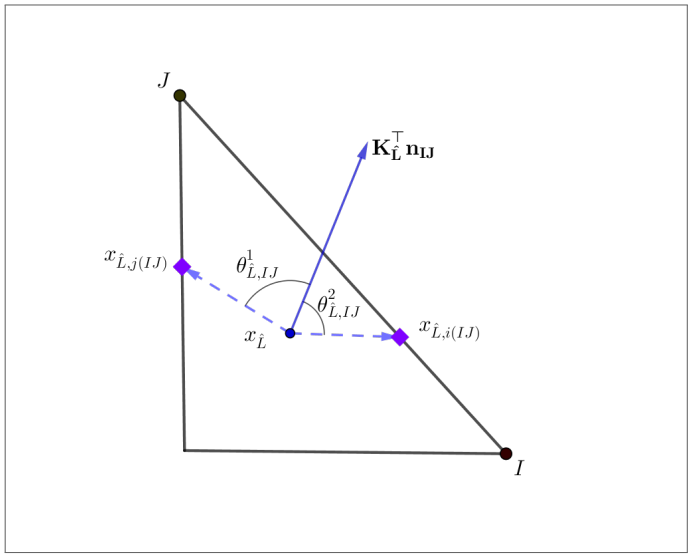

Source: Author.

In these points, $x_{\hat{L},i(IJ)}$ and $x_{\hat{R},i(IJ)}$, such that $x_{\hat{L},i(IJ)} = x_{\hat{R},i(IJ)}$, the coefficients $b_{\hat{L}}$ and $b_{\hat{R}}$ depends solely on physical-geometrical parameters of the domain (GAO; WU, 2013), and $a_{\hat{L}}$ and $a_{\hat{R}}$, in Equation 3.8 and Equation 3.9, respectively, are given by:

$$a_{\hat{L}} = \frac{K^{(n)}_{\hat{L},IJ}}{h_{\hat{L},IJ}}, \quad a_{\hat{R}} = \frac{K^{(n)}_{\hat{R},IJ}}{h_{\hat{R},IJ}}, \quad K^{(n)}_{\hat{L},IJ} = \mathbf{n}_{\mathbf{IJ}}^{\top}\mathbf{K}_{\hat{\mathbf{L}}} \cdot \mathbf{n_{IJ}} \quad \text{and} \quad K^{(n)}_{\hat{R},IJ} = \mathbf{n}_{\mathbf{JI}}^{\top}\mathbf{K}_{\hat{\mathbf{R}}} \cdot \mathbf{n_{JI}} \tag{3.10}$$

where $h_{\hat{L},IJ}$ and $h_{\hat{R},IJ}$ are the orthogonal distances from the correspondents centroids, $x_{\hat{L}}$ and $x_{\hat{R}}$, respectively, to the face IJ, as it can be seen on Figure 4.

Figure 4 – Geometric parameters for a general face (edge in 2-D) of two adjacent control volumes $\hat{L}$ and $\hat{R}$.

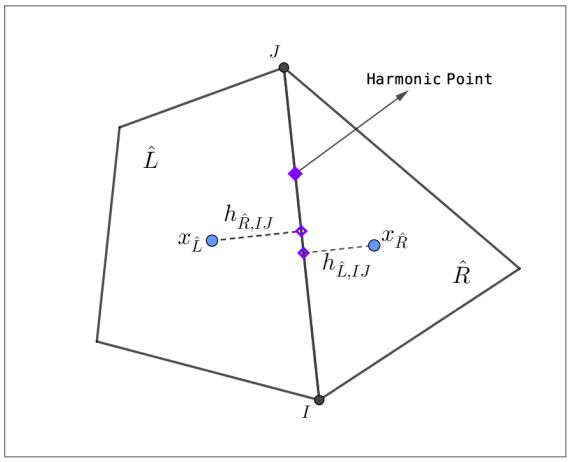

Source: Author.

Subtracting Equation 3.9 from Equation 3.8 and isolating the harmonic point, $x_{\hat{L},i(IJ)}$, as a function of the physical and geometrical parameters, leads us to the following expression:

$$x_{\hat{L},i(IJ)} = \frac{a_{\hat{L}} x_{\hat{L}} + a_{\hat{R}} x_{\hat{R}} + \left(\mathbf{K}_{\hat{\mathbf{L}}}^{\top} - \mathbf{K}_{\hat{\mathbf{R}}}^{\top}\right) \mathbf{n_{IJ}}}{a_{\hat{L}} + a_{\hat{R}}} + \frac{b_{\hat{R}}(J-I) - b_{\hat{L}}(I-J)}{a_{\hat{L}} + a_{\hat{R}}} \tag{3.11}$$

substituting the values of the parameters $a_{\hat{L}}$ and $a_{\hat{R}}$ given by Equation 3.10 in Equation 3.11, we obtain:

$$x_{\hat{L},i(IJ)} = \frac{h_{\hat{L},IJ} K_{\hat{R},IJ}^{(n)} x_{\hat{R}} + h_{\hat{R},IJ} K_{\hat{L},IJ}^{(n)} x_{\hat{L}} + h_{\hat{L},IJ} h_{\hat{R},IJ} \left(\mathbf{K}_{\hat{\mathbf{L}}}^{\top} - \mathbf{K}_{\hat{\mathbf{R}}}^{\top}\right) \mathbf{n_{IJ}}}{h_{\hat{L},IJ} K_{\hat{R},IJ}^{(n)} + h_{\hat{R},IJ} K_{\hat{L},IJ}^{(n)}} + \frac{h_{\hat{L},IJ} h_{\hat{R},IJ} \left(b_{\hat{R}} - b_{\hat{L}}\right)(J-I)}{h_{\hat{L},IJ} K_{\hat{R},IJ}^{(n)} + h_{\hat{R},IJ} K_{\hat{L},IJ}^{(n)}} \tag{3.12}$$

Figure 5 – Stencil for the discrete flux on the control surface using harmonic interpolation points.

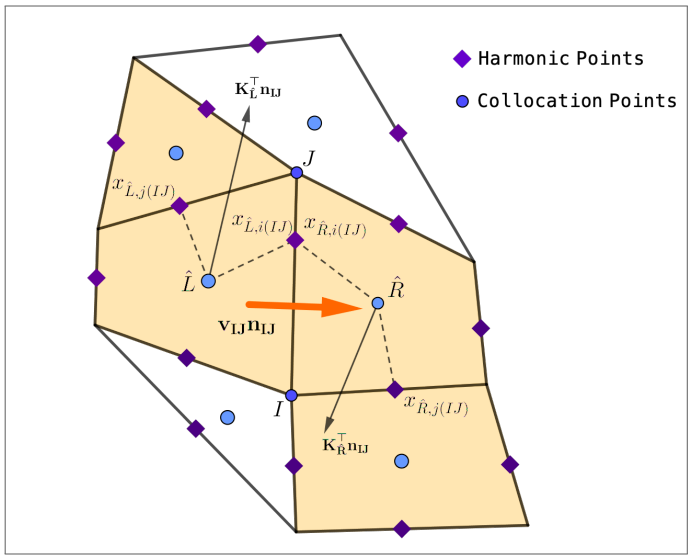

Source: Author.

A sufficient condition to derive a method with a local stencil, is given by assuming $b_{\hat{L}} = b_{\hat{R}}$ (GAO; WU, 2013). Thus, by making this assumption, we have:

$$x_{\hat{L},i(IJ)} = \frac{h_{\widehat{L},IJ} k^{(n)}_{\widehat{R},IJ} x_{\widehat{R}} + h_{\widehat{R},IJ} k^{(n)}_{\widehat{L},IJ} x_{\widehat{L}} + h_{\widehat{L},IJ} h_{\widehat{R},IJ} \left(\mathbf{K}^{\top}_{\widehat{L}} - \mathbf{K}^{\top}_{\widehat{R}}\right) \mathbf{n}_{IJ}}{h_{\widehat{L},IJ} k^{(n)}_{\widehat{R},IJ} + h_{\widehat{R},IJ} k^{(n)}_{\widehat{L},IJ}} \tag{3.13}$$

Similarly, following the same procedure, we can define the harmonic point $x_{\hat{L},j(IJ)}$ and $x_{\hat{R},j(IJ)}$. For control surfaces inside the domain, the interpolation point defined in Equation 3.13 is the harmonic point for a non-homogeneous porous media. On the other hand, if the control surface that belongs to the boundary of the domain we simply use the middle point of the face IJ as the interpolation point (CONTRERAS, 2016).

Remark. *When dealing with severely distorted meshes or with problems that presents high anisotropy, the harmonic points even belonging to the face (edge in 2-D) IJ, the sum of the angles $\theta^1_{\hat{L},IJ} + \theta^2_{\hat{L},IJ}$ is greater than $180°$, in this case we adopted the middle point of the face as the harmonic point (see Figure 6) (CONTRERAS et al., 2017).*

Figure 6 – Representation of a pathological case in which the harmonic point belongs to the edge, but the sum the angles is greater than $180°$.

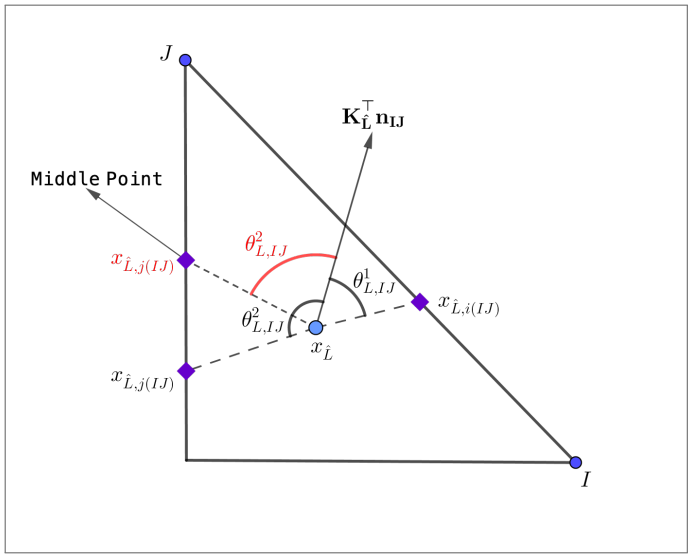

Source: Author.

A particular case for the harmonic points calculation arises when dealing with a homogeneous and isotropic porous media such as inside the vuggy region (free flow region). In this scenario, the harmonic points, $x_{\hat{L},i(IJ)}$ and $x_{\hat{L},j(IJ)}$ only depend on geometric parameters of the two adjacents control volumes $\hat{L}$ and $\hat{R}$, then:

$$x_{\hat{L},i(IJ)} = \frac{h_{\widehat{L},IJ} x_{\widehat{L}} + h_{\widehat{R},IJ} x_{\widehat{R}}}{h_{\widehat{L},IJ} + h_{\widehat{R},IJ}} \tag{3.14}$$

Once the interpolation points are defined for all control surfaces of the computational mesh, the value of the variables at these points can be computed as a convex combination of the cell center variables regarding the control volumes that shared a generic face IJ of the domain, as given by:

$$p_{IJ} = \omega_{\hat{L},IJ} p_{\widehat{L}} + \omega_{\hat{R},IJ} p_{\widehat{R}} \tag{3.15}$$

where $\omega_{\hat{L},IJ}$ and $\omega_{\hat{L},IJ}$ are the weights defined in Equation 3.16. It should be pointed out that the interpolation given by Equation 3.15 fulfills the linearity-preserving criteria (CONTRERAS, 2016).

$$\omega_{\hat{L},IJ} = \frac{h_{\hat{R},IJ}\, k^{(n)}_{\hat{L},IJ}}{h_{\hat{R},IJ}\, k^{(n)}_{\hat{L},IJ} + h_{\hat{L},IJ}\, k^{(n)}_{\hat{R},IJ}} \qquad \text{and} \qquad \omega_{\hat{R},IJ} = 1 - \omega_{\hat{L},IJ} \tag{3.16}$$

3.2.2 Diffusive Term

Considering the third term in the left hand side of Equation 3.5, we can write as:

$$-\sum_{i=1}^{n_v} \int_{\Omega_{\hat{L}}} \nabla \cdot (\mu \nabla \mathbf{u})\, d\Omega_{\hat{L}} = \sum_{i=1}^{n_v} \int_{\Omega_{\hat{L}}} \nabla \cdot \mathbf{F}\, d\Omega_{\hat{L}} \tag{3.17}$$

in which $\mathbf{F} = -\boldsymbol{\mathcal{M}} \nabla \mathbf{u}$ is the diffusive flux flux and $\boldsymbol{\mathcal{M}} = \mu \mathbf{I}$, where $\mathbf{I}$ is identity matrix. Applying the Green-Gauss divergence theorem in Equation 3.17, considering a generic control volume $\hat{L}$, we get:

$$\int_{\Omega_{\hat{L}}} \nabla \cdot \mathbf{F}\, d\Omega_{\hat{L}} = \int_{\Gamma_{\hat{L}}} \mathbf{F} \cdot \mathbf{n}_{\Gamma_{\hat{L}}}\, d\Gamma_{\hat{L}} = \sum_{IJ \in \Gamma_{\hat{L}}} \int_{IJ} \mathbf{F} \cdot \mathbf{n_{IJ}} ds \tag{3.18}$$

Now consider two control volumes, namely $\hat{R}$ and $\hat{L}$, adjacent to a generic internal face IJ of the domain Ω, see Fig 5. We can define the one-sided flux of a given property ϕ with respect to the control volume $\hat{L}$ for a face IJ of $\Gamma_{\hat{L}}$ as:

$$\int_{IJ} \mathbf{F} \cdot \mathbf{n_{IJ}}\, d\Gamma_{\hat{L}} = \int_{IJ} -\boldsymbol{\mathcal{M}}_{\hat{L}} \nabla \phi \ \cdot \mathbf{n_{IJ}}\, ds = \mathbf{F}^{\hat{L}}_{\phi,IJ} \cdot \mathbf{N_{IJ}}, \quad \text{with} \quad \phi = u \text{ or } v \tag{3.19}$$

where $\mathbf{F}^{\hat{L}}_{\phi,IJ} = -\boldsymbol{\mathcal{M}}_{\hat{L}} (\nabla \phi)_{IJ}$, and $\mathbf{N_{IJ}}$ is the area vector of the edge IJ. Now we can rewrite Equation3.19 as:

$$\mathbf{F}^{\hat{L}}_{\phi,IJ} \cdot \mathbf{N_{IJ}} = \int_{IJ} -\boldsymbol{\mathcal{M}}_{\hat{L}} \nabla \phi \cdot \mathbf{n_{IJ}}\, ds = \int_{IJ} -\nabla \phi \cdot \left(\boldsymbol{\mathcal{M}}^{\top}_{\hat{L}} \mathbf{n_{IJ}} \right)\, ds \tag{3.20}$$

in which ϕ represents each of velocity components, u and v of the velocity vector $\mathbf{u}$. In Equation 3.20, we should approximate the term $\nabla \phi \cdot \left(\boldsymbol{\mathcal{M}}^{\top}_{\hat{L}} \mathbf{n_{IJ}} \right)$, using a Taylor series expansion (POTIER, 2009; YUAN; SHENG, 2008).

3.2.2.1 MPFA based in Harmonic points scheme MPFA-H

In this sub section, we describe the Multipoint Flux Approximation mehtod based on harmonic points MPFA-H, which was orginally devised to discretize diffusion problems in heterogeneous and anisotropic media in (GAO; WU, 2014) and that was adapted for modeling Darcian two-phase fluid flows in petroleum reservoirs by (CONTRERAS, 2016; QUEIROZ et al., 2014; CARVALHO; WILLMERSDORF; LYRA, 2009; TEIXEIRA; GUIMARÃES; CARVALHO, 2021). In this scheme, the unique flux on each control surface of the discrete domain is expressed as a linear combination of the one-sided fluxes of the two control volumes adjacent to each face.

These fluxes are explicitly expressed by one cell centered unknown and points defined on the faces that do not necessarily belong to the same face shared by the adjacent cells independently (AGELAS; EYMARD; HERBIN, 2009). In Figure 5, we present a small portion of a polygonal 2-D mesh with the stencil used to define the face fluxes and the harmonic points.

Using the vectors non collinear $x_{\hat{L},i(IJ)}$ and $x_{\hat{L},j(IJ)}$, in a way that the vectors $\overrightarrow{x_{\hat{L}}x_{\hat{L},i(IJ)}}$ and $\overrightarrow{x_{\hat{L}}x_{\hat{L},j(IJ)}}$ are not collinear, as it can be seen in Figure 7. This implies that there are two coefficients $\alpha_{\hat{L},i(IJ)}$ and $\alpha_{\hat{L},j(IJ)}$ associated to each auxiliary point, we can write:

$$\boldsymbol{\mathcal{M}}_{\hat{L}}^{\top}\mathbf{n_{IJ}} = \alpha_{\hat{L},i(IJ)}\,\overrightarrow{x_{\hat{L}}x_{\hat{L},i(IJ)}} + \alpha_{\hat{L},j(IJ)}\,\overrightarrow{x_{\hat{L}}x_{\hat{L},j(IJ)}} \tag{3.21}$$

where $x_{\hat{L}}$ is the centroid of the control volume $\hat{L}$, and the term $\boldsymbol{\mathcal{M}}_{\hat{L}}^{\top}\mathbf{n_{IJ}}$ is the projection of $\mathcal{M}$ in the normal direction of a face IJ. In Equation 3.21 the coefficients $\alpha_{\hat{L},i(IJ)}$ and $\alpha_{\hat{L},j(IJ)}$ are given by:

$$\alpha_{\hat{L},i(IJ)} = \frac{\left(\boldsymbol{\mathcal{M}}_{\hat{L}}^{\top}\mathbf{n_{IJ}}, \overrightarrow{x_{\hat{L}}x_{\hat{L},j(IJ)}}, \vec{e}_z\right)}{\left(\overrightarrow{x_{\hat{L}}x_{\hat{L},i(IJ)}}, \overrightarrow{x_{\hat{L}}x_{\hat{L},j(IJ)}}, \vec{e}_z\right)} \quad \text{and} \quad \alpha_{\hat{L},j(IJ)} = \frac{\left(\overrightarrow{x_{\hat{L}}x_{\hat{L},i(IJ)}}, \boldsymbol{\mathcal{M}}_{\hat{L}}^{\top}\mathbf{n_{IJ}}, \vec{e}_z\right)}{\left(\overrightarrow{x_{\hat{L}}x_{\hat{L},i(IJ)}}, \overrightarrow{x_{\hat{L}}x_{\hat{L},j(IJ)}}, \vec{e}_z\right)} \tag{3.22}$$

where $(\vec{a}, \vec{b}, \vec{c})$ represents the mixed product of the vectors $\vec{a}$, $\vec{b}$, $\vec{c}$, and $\vec{e}_z$ is the unitary vector that represents the z axis.

By substituting Equation 3.21 into Equation 3.20, and using a finite difference method to approximate the partial derivatives of ϕ, i.e. $\nabla\phi$ along the directions, $\overrightarrow{x_{\hat{L}}x_{\hat{L},i(IJ)}}$ and $\overrightarrow{x_{\hat{L}}x_{\hat{L},j(IJ)}}$, we get:

$$\mathbf{F}_{\phi,IJ}^{\hat{L}} \cdot \mathbf{N_{IJ}} = \int_{IJ} -\nabla\phi \cdot \left(\boldsymbol{\mathcal{M}}_{\hat{L}}^{\top}\mathbf{n_{IJ}}\right) ds = \|\vec{IJ}\| \left(\alpha_{\hat{L},i(IJ)} \frac{\phi_{\hat{L}} - \phi_{\hat{L},i(IJ)}}{\|\overrightarrow{x_{\hat{L}}x_{\hat{L},i(IJ)}}\|} + \alpha_{\hat{L},j(IJ)} \frac{\phi_{\hat{L}} - \phi_{\hat{L},j(IJ)}}{\|\overrightarrow{x_{\hat{L}}x_{\hat{L},j(IJ)}}\|}\right) \tag{3.23}$$

Equation 3.23 is equivalent to:

$$\mathbf{F}_{\phi,IJ}^{\hat{L}} \cdot \mathbf{N_{IJ}} = \|\vec{IJ}\| \left(\xi_{\hat{L},i(IJ)}(\phi_{\hat{L}} - \phi_{\hat{L},i(IJ)}) + \xi_{\hat{L},j(IJ)}(\phi_{\hat{L}} - \phi_{\hat{L},j(IJ)})\right) \tag{3.24}$$

Figure 7 – Representation of the physical and geometric parameters for the MPFA-H method for diffusive fluxes.

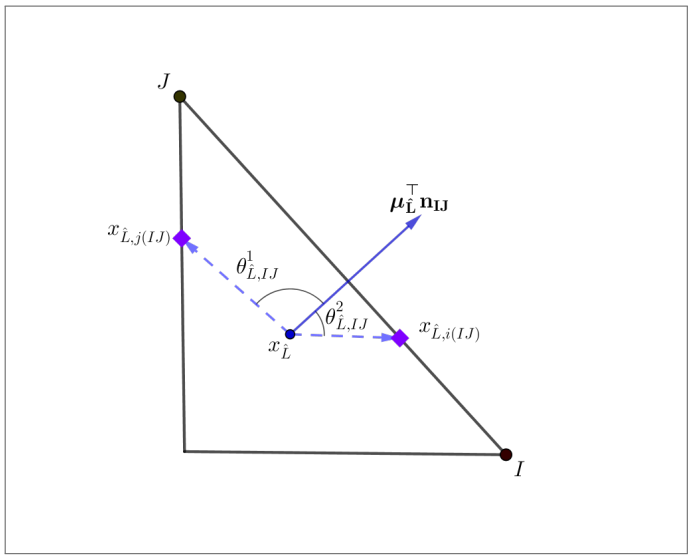

Source: Author.

where:

$$\xi_{\hat{L},i(IJ)} = \frac{\alpha_{\hat{L},i(IJ)}}{\|\overrightarrow{x_{\hat{L}}x_{\hat{L},i(IJ)}}\|} \quad \text{and} \quad \xi_{\hat{L},j(IJ)} = \frac{\alpha_{\hat{L},j(IJ)}}{\|\overrightarrow{x_{\hat{L}}x_{\hat{L},j(IJ)}}\|} \tag{3.25}$$

Similarly, for the control volume $\hat{R}$ it is possible to write the one-sided flux with respect to the face IJ, as:

$$\mathbf{F}^{\hat{R}}_{\phi,IJ} \cdot \mathbf{N_{IJ}} = \|\vec{IJ}\| \left(\xi_{\hat{R},i(IJ)}(\phi_{\hat{R}} - \phi_{\hat{R},i(IJ)}) + \xi_{\hat{R},j(IJ)}(\phi_{\hat{R}} - \phi_{\hat{R},j(IJ)})\right) \tag{3.26}$$

where:

$$\xi_{\hat{R},i(IJ)} = \frac{\alpha_{\hat{R},i(IJ)}}{\|\overrightarrow{x_{\hat{R}}x_{\hat{R},i(IJ)}}\|} \quad \text{and} \quad \xi_{\hat{R},j(IJ)} = \frac{\alpha_{\hat{R},j(IJ)}}{\|\overrightarrow{x_{\hat{R}}x_{\hat{R},j(IJ)}}\|} \tag{3.27}$$

In Equation 3.27, and as shown on Figure 7, $x_{\hat{R}}$ is the centroid of the control volume $\hat{R}$, and $x_{\hat{R},i(IJ)}$, $x_{\hat{R},j(IJ)}$ are the interpolations points related to the control volume $\hat{R}$.

In order to obtain a conservative scheme, the unique flux over the face IJ is written as a convex combination of the one-sided fluxes (FUHRMANN; OHLBERGER; ROHDE, 2014), given by Equation 3.24 and Equation 3.26:

$$\mathbf{F}_{\phi,IJ} \cdot \mathbf{N_{IJ}} = w_{\hat{L},IJ}\mathbf{F}^{\hat{L}}_{\phi,IJ} \cdot \mathbf{N_{IJ}} + w_{\hat{R},IJ}\mathbf{F}^{\hat{R}}_{\phi,IJ} \cdot \mathbf{N_{IJ}} \tag{3.28}$$

in which $w_{\hat{L},IJ}$ and $w_{\hat{R},IJ}$ are weights, defined as:

$$w_{\hat{L},IJ} = \frac{h_{\hat{R},IJ}}{h_{\hat{R},IJ} + h_{\hat{L},IJ}} \qquad and \qquad w_{\hat{R},IJ} = 1 - w_{\hat{L},IJ} \tag{3.29}$$

where $h_{\hat{L},IJ}$ (resp. $h_{\hat{R},IJ}$) is the orthogonal distance from $x_{\hat{L}}$ (resp. $x_{\hat{R}}$) to the face IJ (see Figure 4). Importantly, in Equation 3.29, the weights depends only on geometrical parameters and they satisfy the convex restriction condition $w_{\hat{R},IJ} + w_{\hat{L},IJ} = 1$ (POTIER, 2009; LIPNIKOV et al., 2007; CONTRERAS, 2016). After some algebraic manipulation (CONTRERAS, 2016), the total flux of a face IJ can then be written as:

$$\mathbf{F}_{\phi,IJ} \cdot \mathbf{N_{IJ}} = \sum_{\gamma=i,j} \sum_{\hat{r}=\hat{L},\hat{R}} \chi_{\hat{r},\gamma(IJ)}(\phi_{\hat{r}} - \phi_{\hat{r},\gamma(IJ)}) \|\vec{IJ}\| \tag{3.30}$$

where $\chi_{\hat{r},\gamma(IJ)} = w_{\hat{r},IJ}\xi_{\hat{r},\gamma(IJ)}$, with $\hat{r} = \hat{L}, \hat{R}$ and $\gamma = i, j$.

Then, the velocities components on the harmonic points given by Equation 3.14 are defined as: $\phi_{\hat{r},\gamma(IJ)} = \omega_{\hat{M},\gamma(IJ)}\phi_{\widehat{M},\gamma} + \omega_{\hat{N},\gamma(IJ)}\phi_{\widehat{N},\gamma}$, where $\omega_{\hat{M},\gamma IJ} = \frac{h_{\widehat{M},\gamma(IJ)}}{h_{\widehat{M},\gamma(IJ)} + h_{\widehat{N},\gamma(IJ)}}$ and $\omega_{\hat{N},(IJ)} = 1 - \omega_{\hat{M},\gamma(IJ)}$, in which M and N are the two control volumes that sharing a generic face IJ.

3.2.3 Darcy Term

The so called Darcy term in this work, refers to the second term in Equation 3.5. Thus, consider a generic control volume $\hat{L}$, with respective permeability tensor $\mathbf{K_{\hat{L}}}$. By integrating, over a generic control volume $\hat{L}$ and by using the mean value theorem, we get:

$$\int_{\Omega_{\hat{L}}} \mu \mathbf{K_{\hat{L}}^{-1}} \mathbf{u} \, d\Omega_{\hat{L}} = \mu V_{\hat{L}} \mathbf{K_{\hat{L}}^{-1}} \mathbf{u_{\hat{L}}^{n+1}} \tag{3.31}$$

in which $\mathbf{u}_{\hat{L}} = \frac{1}{V_{\hat{L}}} \int \mathbf{u} dV$ in $\Omega_{\hat{L}}$, with $V_{\hat{L}}$ being the volume (area in 2-D) of the control volume $\hat{L}$.

3.2.4 Transient Term

We use the first order Euler backward scheme to approximate the transient term , first term in Equation 3.5. Which considering a generic control volume $\hat{L}$ as:

$$\int_{\Omega_{\hat{L}}} \rho \frac{\partial \mathbf{u}}{\partial t} \, d\Omega_{\hat{L}} = \frac{\rho V_{\hat{L}}}{\Delta t} \left({\mathbf{u}_{\hat{\mathbf{L}}}}^{n+1} - {\mathbf{u}_{\hat{\mathbf{L}}}}^{n} \right) \tag{3.32}$$

in which Δt is the time step, $\Delta t = t^{n+1} - t^n$, and the superscripts $n+1$ and n refer, to the next and the current time level of the simulation, respectively. In this thesis, we have adopted a fully implicit scheme, in other words, all the variables, pressure and velocity, are evaluated at the time step $n+1$.

3.2.5 Final Form of the Momentum Equation

After the discretization of all terms in Equation 3.5 using the MPFA-H scheme, considering a generic control volume $\hat{L}$ we get:

$$\frac{\rho V_{\hat{L}}}{\Delta t}\left({\phi_{\hat{L}}}^{n+1} - {\phi_{\hat{L}}}^{n}\right) + \mu V_{\hat{L}}\mathbf{K}_{\hat{\mathbf{L}}}^{-\mathbf{1}}\phi_{\hat{L}}^{n+1} + \sum_{\Gamma_{IJ}\in\Gamma_{\hat{L}}}\sum_{\gamma=i,j}\sum_{\hat{r}=\hat{L},\hat{R}}\|\vec{IJ}\|\chi_{\hat{r},\gamma(IJ)}(\phi_{\hat{r}} - \phi_{\hat{r},\gamma(IJ)})^{n+1} = -\sum_{\Gamma_{IJ}\in\Gamma_{\hat{L}}} p_{IJ}^{n+1}\|IJ\|\mathbf{n}_{IJ} \quad (3.33)$$

Grouping all terms related to the velocity components and to the pressure gradient, we can write the equations for the conservation of momentum in a more compact form, as:

$$a_{u,\hat{L}}u_{\hat{L}}^{n+1} = \sum_{i=1}^{nb}(a_{u,nb}u_{nb})_P^{n+1} - V_{\hat{L}}\left(\frac{\partial p}{\partial x}\right)_{\hat{L}}^{n+1} + \frac{\rho_{\hat{L}}V_{\hat{L}}}{\Delta t}u_{\hat{L}}^{n} \quad (3.34)$$

$$a_{v,\hat{L}}v_{\hat{L}}^{n+1} = \sum_{i=1}^{nb}(a_{v,nb}v_{nb})_P^{n+1} - V_{\hat{L}}\left(\frac{\partial p}{\partial y}\right)_{\hat{L}}^{n+1} + \frac{\rho_{\hat{L}}V_{\hat{L}}}{\Delta t}v_{\hat{L}}^{n} \quad (3.35)$$

where,

$$a_{u,\hat{L}} = \frac{\rho V_{\hat{L}}}{\Delta t} + \mu V_{\hat{L}}\mathbf{K}_{\hat{\mathbf{L}}}^{-\mathbf{1}} + \sum_{\Gamma_{IJ}\in\Gamma_{\hat{L}}}\left(\sum_{\gamma=i,j}\chi_{\hat{L},\gamma(IJ)}(1+\omega_{\hat{L},\gamma(IJ)})) - \omega_{\hat{R},j(IJ)}\right)\|\vec{IJ}\| \quad (3.36)$$

$$a_{u,nb} = \sum_{\Gamma_{IJ}\in\Gamma_{\hat{L}}}\left(\sum_{\gamma=i,j}\chi_{\hat{L},\gamma(IJ)}(1+\omega_{\hat{R},\gamma(IJ)})) - \omega_{\hat{L},j(IJ)}\right)\|\vec{IJ}\| \quad (3.37)$$

and,

$$a_{v,\hat{L}} = \frac{\rho V_{\hat{L}}}{\Delta t} + \mu V_{\hat{L}}\mathbf{K}_{\hat{\mathbf{L}}}^{-\mathbf{1}} + \sum_{\Gamma_{IJ}\in\Gamma_{\hat{L}}}\left(\sum_{\gamma=i,j}\chi_{\hat{L},\gamma(IJ)}(1+\omega_{\hat{L},\gamma(IJ)})) - \omega_{\hat{R},j(IJ)}\right)\|\vec{IJ}\| \quad (3.38)$$

$$a_{v,nb} = \sum_{\Gamma_{IJ}\in\Gamma_{\hat{L}}}\left(\sum_{\gamma=i,j}\chi_{\hat{L},\gamma(IJ)}(1+\omega_{\hat{R},\gamma(IJ)})) - \omega_{\hat{L},j(IJ)}\right)\|\vec{IJ}\| \quad (3.39)$$

in which, adopting the classical and more compact form of representing the discrete equations, $a_{u,\hat{L}}$ is the central coefficient, related to the u component of the velocity at the control volume $\hat{L}$, and $a_{u,nb}$ are the coefficients connecting the variables at the cell center with their respective neighbors. Whenever dealing with structured meshes, those neighbors are normally refereed to n, s, e, w, north, south, east and west (PATANKAR, 2018). Furthermore, $\rho_{\hat{L}}$ is the fluid density on the control volume $\hat{L}$, once the fluid flow is considered incompressible, this value is constant throughout the whole simulation.

Since we have adopted a cell centered variable arrangement the coefficients $a_{u,\hat{L}}$ and $a_{u,nb}$ are the same as $a_{v,\hat{L}}$ and $a_{v,nb}$ in Equation 3.34 and Equation 3.35, but with different pressure gradient and transient terms.

3.2.6 Mass Conservation Equation

Considering the Equation 3.6 for a generic control volume $\hat{L}$ and apllying the Green-Gauss divergence theorem:

$$\int_{\Omega_{\hat{L}}} \nabla \cdot \mathbf{u}\, d\Omega_{\hat{L}} = \int_{\Gamma_{\hat{L}}} \mathbf{u}\, d\Gamma_{\hat{L}} = \sum_{\Gamma_{IJ} \in \Gamma_{\hat{L}}} (\mathbf{u}_{IJ} \mathbf{n}_{IJ} \|IJ\|) \tag{3.40}$$

in which $\mathbf{u}_{IJ}$ is the cell face velocity.

If a central difference scheme is adopted to approximate the control surfaces velocities, it is well know in literature that a decoupling between the pressure and velocity variables may occur (PATANKAR, 2018) spurious oscillatory pressure fields may arise. In order to guarantee the proper coupling between the variables, different strategies are used to approximate the control surface velocities such as: the Rhie-Chow interpolation method (RHIE; CHOW, 1983), the momentum interpolation method, proposed by Majumdar (1988), and the Physical Influence Scheme (SCHNEIDER; RAW, 1987).

In the present thesis a modification of the original Rhie and Chow interpolation (RHIE; CHOW, 1983) is used. In this new scheme, proposed by (ZHANG; ZHAO; BAYYUK, 2014), the well know problems of the Rhie and Chow interpolation, for example the time step dependence and the large errors due the presence of strong body forces, are addressed and solved.

3.2.6.1 Momentum Interpolation Scheme

Considering two generic control volumes adjacent to the same control surface IJ (edge in 2-D) of the computational mesh, namely $\hat{L}$ and $\hat{R}$. We can write the momentum equations for the velocity component u such as Equation 3.34:

$$a_{u,\hat{L}} u_{\hat{L}}^{n+1} = \sum_{i=1}^{nb} (a_{u,nb} u_{nb})_{\hat{L}}^{n+1} - V_{\hat{L}} \left(\frac{\partial p}{\partial x} \right)_{\hat{L}}^{n+1} + \frac{\rho_{\hat{L}} V_{\hat{L}}}{\Delta t} u_{\hat{L}}^{n} \tag{3.41}$$

$$a_{u,\hat{R}} u_{\hat{R}}^{n+1} = \sum_{i=1}^{nb} (a_{u,nb} u_{nb})_{\hat{R}}^{n+1} - V_{\hat{R}} \left(\frac{\partial p}{\partial x} \right)_{\hat{R}}^{n+1} + \frac{\rho_{\hat{R}} V_{\hat{R}}}{\Delta t} u_{\hat{R}}^{n} \tag{3.42}$$

where, $V_{\hat{R}}$ is the volume (area in 2-D) of the control volume $\hat{R}$ and $\rho_{\hat{R}}$ is the fluid density on the control volume $\hat{R}$.

Similarly, we can write for the face IJ:

$$a_{u,IJ} u_{IJ}^{n+1} = \sum_{i=1}^{nb} (a_{u,nb} u_{nb})_{IJ}^{n+1} - V_{IJ} \left(\frac{\partial p}{\partial x} \right)_{IJ}^{n+1} + \frac{\rho_{IJ} V_{IJ}}{\Delta t} u_{IJ}^{n} \tag{3.43}$$

In order to derive the Rhie-Chow interpolation, we need to define the following auxiliary variables:

$$M_{u,i} = \frac{\sum_{i=1}^{nb}(a_{u,nb}u_{nb})_i^{n+1}}{a_{u,i}} \qquad and \qquad i = \hat{L}, \hat{R}, IJ \tag{3.44}$$

Considering that, $M_{u,IJ}$ can be obtained by a linear interpolation between the values of the control volumes at the left and at the right side of the face IJ, we can write:

$$M_{u,IJ} = (1-\beta)M_{u,\hat{L}} + \beta M_{u,\hat{R}} \tag{3.45}$$

in this work, we have adopted $\beta = \frac{1}{2}$, similarly as in the original MIM proposed by Rhie and Chow (1983).

Substituting the terms $M_{u,\hat{L}}$ and $M_{u,\hat{R}}$ in Equation 3.45, and rearranging the terms, the control surface velocities can be expressed as:

$$u_{IJ} = \overline{u_{IJ}} + \frac{(1-\beta)V_{\hat{L}}}{a_{u,\hat{L}}}\left(\frac{\partial p}{\partial x}\right)_{\hat{L}}^{n+1} + \frac{\beta V_{\hat{R}}}{a_{u,\hat{R}}}\left(\frac{\partial p}{\partial x}\right)_{\hat{R}}^{n+1} - \frac{V_{IJ}}{a_{u,IJ}}\left(\frac{\partial p}{\partial x}\right)_{IJ}^{n+1} + (\textit{TRANSIENT TERM}) \tag{3.46}$$

in which:

$$\frac{V_{IJ}}{a_{u,IJ}} = \frac{(1-\beta)V_{\hat{L}}}{a_{u,\hat{L}}} + \frac{\beta V_{\hat{R}}}{a_{u,\hat{R}}} \tag{3.47}$$

and:

$$\overline{u_{IJ}} = (1-\beta)u_{\hat{L}}^{n+1} + \beta u_{\hat{R}}^{n+1} \tag{3.48}$$

3.2.6.2 Transient term interpolation

In order to overcome the well know problems of the conventional Rhie-Chow interpolation scheme when dealing with small time steps, we have decided to use the method proposed by (ZHANG; ZHAO; BAYYUK, 2014). Therefore, we can write the transient term as:

$$\textit{TRANSIENT TERM} = -\frac{(1-\beta)\rho_{\hat{L}}V_{\hat{L}}}{a_{u,\hat{L}}\,\Delta t}u_{\hat{L}}^{n} - \frac{\beta\rho_{\hat{R}}V_{\hat{R}}}{a_{u,\hat{R}}\,\Delta t}u_{\hat{R}}^{n} + \frac{\rho_{IJ}V_{IJ}}{a_{u,IJ}\,\Delta t}u_{IJ}^{n} \tag{3.49}$$

where it is feasible to make the following approximations (ZHANG; ZHAO; BAYYUK, 2014):

$$\frac{\rho_{\hat{L}}V_{\hat{L}}}{a_{u,\hat{L}}\,\Delta t} \approx \frac{\rho_{IJ}V_{IJ}}{a_{u,IJ}\,\Delta t} \tag{3.50}$$

$$\frac{\rho_{\hat{R}}V_{\hat{R}}}{a_{u,\hat{R}}\,\Delta t} \approx \frac{\rho_{IJ}V_{IJ}}{a_{u,IJ}\,\Delta t} \tag{3.51}$$

by doing that, the cell face velocity, Equation 3.46, can be written as:

$$u_{IJ} = \overline{u_{IJ}} + \frac{(1-\beta)V_{\hat{L}}}{a_{u,\hat{L}}}\left(\frac{\partial p}{\partial x}\right)_{\hat{L}}^{n+1} + \frac{\beta V_{\hat{R}}}{a_{u,\hat{R}}}\left(\frac{\partial p}{\partial x}\right)_{\hat{R}}^{n+1} - \frac{V_{IJ}}{a_{u,IJ}}\left(\frac{\partial p}{\partial x}\right)_{IJ}^{n+1} + \frac{\rho_{IJ}V_{IJ}}{a_{u,IJ}\,\Delta t}u_{IJ}^{n} \tag{3.52}$$

where

$$u_{IJ}^{n} = \left[\frac{(1-\beta)V_{\hat{L}}}{a_{u,\hat{L}}} \left(\frac{\partial p}{\partial x} \right)_{\hat{L}} + \frac{\beta V_{\hat{R}}}{a_{u,\hat{R}}} \left(\frac{\partial p}{\partial x} \right)_{\hat{R}} - \frac{V_{IJ}}{a_{u,IJ}} \left(\frac{\partial p}{\partial x} \right)_{IJ} \right]^{n} \tag{3.53}$$

Similarly, following the same procedure, we can write the cell face velocity component v as:

$$v_{IJ} = \overline{v_{IJ}} + \frac{(1-\beta)V_{\hat{L}}}{a_{u,\hat{L}}} \left(\frac{\partial p}{\partial y} \right)_{\hat{L}}^{n+1} + \frac{\beta V_{\hat{R}}}{a_{v,\hat{R}}} \left(\frac{\partial p}{\partial y} \right)_{\hat{R}}^{n+1} - \frac{V_{IJ}}{a_{v,IJ}} \left(\frac{\partial p}{\partial y} \right)_{IJ}^{n+1} + \frac{\rho_{IJ} V_{IJ}}{a_{v,IJ}\,\Delta t} v_{IJ}^{n} \tag{3.54}$$

where

$$v_{IJ}^{n} = \left[\frac{(1-\beta)V_{\hat{L}}}{a_{v,\hat{L}}} \left(\frac{\partial p}{\partial y} \right)_{\hat{L}} + \frac{\beta V_{\hat{R}}}{a_{v,\hat{R}}} \left(\frac{\partial p}{\partial y} \right)_{\hat{R}} - \frac{V_{IJ}}{a_{v,IJ}} \left(\frac{\partial p}{\partial y} \right)_{IJ} \right]^{n} \tag{3.55}$$

By making this assumption, the term depicted in Equation 3.53 becomes larger as the time step decreases, reinforcing the stabilizing effects of these terms.

4 SOLUTION METHODS FOR THE STOKES-BRINKMAN EQUATION

Several strategies have been devised to overcome the numerical difficult for solving mathematical model such as, Navier-Stokes Equations (STOKES, 1845), Stokes-Brinkman Equations (BRINKMAN, 1949), that arises due the coupling between the pressure and velocity variables (AGUERRE et al., 2020). These strategies can be classified in two groups: monolithic and segregated methods.

Monolithic methods solve all the governing equations, conservation of momentum and mass conservation equation, simultaneously for all the variables. Segregated algorithms, on the contrary, solve the equations in a sequencial process, each variable at time (MAZUMDER, 2015; MAZHAR, 2002; FERZIGER; PERIĆ; STREET, 2020).

In this chapter, we present the two methods for solving the Stokes-Brinkman equations. First, the monolithic approach will be discussed, then we will introduce a segregated algorithm to solve the Stokes-Brinkman system of equation using a pressure-velocity coupling algorithm.

4.1 MONOLITHIC APPROACH TO SOLVE THE STOKES-BRINKMAN EQUATION

In Chapter 3 the mass conservation equation and the linear momentum equation were discretized, including the evaluation of the cell face velocities using a modified momentum interpolation scheme. Therefore, the resulting equations will only depend on the cell centered values of the unknowns of the problem.

Unlike the segregated methods, that will be discussed on the following section, when adopting a monolithic approach to solve the system of equation, Equation 4.1, the pressure and velocity fields, obtained during the solution procedure, satisfy both the mass conservation equation and the momentum conservation equation. In fact, the problems that arises from the coupling between the variables p and v is absent when adopting this procedure, once it is implicitly treated during the solution (HONÓRIO, 2013).

$$\begin{matrix} MCE \longrightarrow \\ LMC_x \longrightarrow \\ LMC_y \longrightarrow \end{matrix} \begin{bmatrix} A^{pp} & A^{pu} & A^{pv} \\ A^{up} & A^{uu} & 0 \\ A^{vp} & 0 & A^{vv} \end{bmatrix} \begin{bmatrix} p \\ u \\ v \end{bmatrix} = \begin{bmatrix} B^p \\ B^u \\ B^v \end{bmatrix} \tag{4.1}$$

In Equation 4.1, the linear system of equation has a dimension of $(3n_v \times 3n_v)$, and we can divided it in three sectors. The first one with dimension of $(n_v \times n_v)$, whose coefficients A^{pp},

A^{pu}, A^{pu} and B^{p} arises from the discretization of the mass conservation equation (MCE) using a modified Rhie-Chow interpolation. The second and the third sector refers, respectively, to the linear momentum conservation in the x direction (LMC_x) and in the y direction (LMC_y), both with dimension of $(n_v \times n_v)$, with respective coefficients A^{up} (resp. A^{vp}) , A^{uu} (resp. A^{vv}) and B^{v} (resp. B^{v}). The solution procedure for the monolithic approach can be seen in Figure 8, for the transient regime. It is important to mention that the solution for the permanent regime is only a particular case of the transient regime for a time level in which a steady state is reached.

Figure 8 – Monolithic Flowchart.

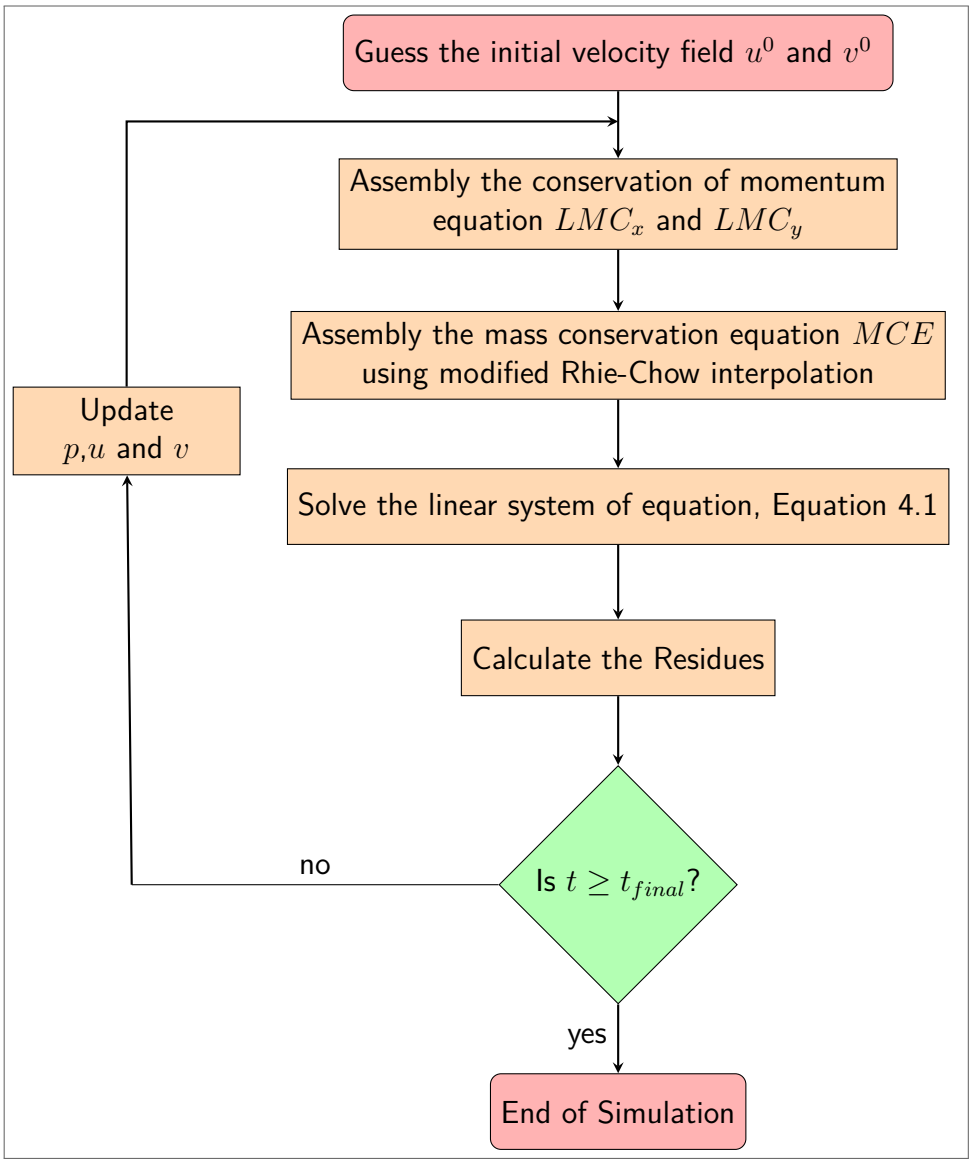

Source: Author.

4.2 SEGREGATED APPROACH TO SOLVE THE STOKES-BRINKMAN EQUATION

Within the so called segregated methods, the penalty method (TEMAM, 1968), the artificial compressibility method (HARTEN, 1978) and the projection method (CHORIN, 1968; CHORIN, 1997) are amidst the most used in Computational Fluid Dynamics (CFD) codes (WANG et al., 2018).

In the projection methods, an initial estimation of the velocity field is corrected as a result of a pressure equation in which the velocity field is enforced to satisfy the divergence free-condition. Specifically, the Fractional Step Method (KIM; MOIN, 1985) count on a temporal splitting on the velocity field: first an intermediate velocity is obtained with the conservation of momentum equation using a guessed pressure field, this velocity is subsequently corrected by solving a pressure correction equation based on the mass conservation.

Under the context of projection methods, a family of pressure-velocity algorithms known as SIMPLE-like algorithms, was originally introduced with the development of Semi Implicit Linked Equations (SIMPLE) proposed by Patankar and Spalding (1983). In this scheme, a pressure equation is derived after introducing the momentum equation into the mass conservation equation. A drawback to use a procedure similar to the SIMPLE algorithm to solve the Stokes-Brinkman equation, is that it does not "see" the porous media (ČIEGIS; ILIEV; LAKDAWALA, 2007).

Another approach is the SIMPLEC algorithm, proposed by Doormaal and Raithby (1984), in which the neighbours velocity correction are equal to the one of the current cell. By making this assumption, there is no need to under relax the pressure field. The SIMPLEC algorithm adopted in this work can be described as follows:

The conservation of momentum equation, for a generic control volume $\hat{L}$, can be written as:

$$a_{u,\hat{L}} u_{\hat{L}}^{n+1} = \sum_{i=1}^{nb} (a_{u,nb} u_{nb})_{\hat{L}}^{n+1} - V_{\hat{L}} \left(\frac{\partial p}{\partial x} \right)_{\hat{L}}^{n+1} + \frac{\rho V_{\hat{L}}}{\Delta t} u^n \tag{4.2}$$

$$a_{v,\hat{L}} v_{\hat{L}}^{n+1} = \sum_{i=1}^{nb} (a_{v,nb} v_{nb})_{\hat{L}}^{n+1} - V_{\hat{L}} \left(\frac{\partial p}{\partial y} \right)_{\hat{L}}^{n+1} + \frac{\rho V_{\hat{L}}}{\Delta t} v^n \tag{4.3}$$

The first step in the SIMPLEC algorithm uses a guessed pressure field, p^*, to estimate an intermediate velocity field, u^* and v^*, that does not necessarily satisfy both the conservation of momentum and the mass conservation equation. By using Equations 4.2 and 4.3, it follows

that:

$$a_{u,\hat{L}}u^*_{\hat{L}} = \sum_{i=1}^{nb}(a_{u,nb}u^*_{nb})_{\hat{L}} - V_{\hat{L}}\left(\frac{\partial p^*}{\partial x}\right)_{\hat{L}} + \frac{\rho V_{\hat{L}}}{\Delta t}u^n \tag{4.4}$$

$$a_{v,\hat{L}}u^*_{\hat{L}} = \sum_{i=1}^{nb}(a_{v,nb}v^*_{nb})_{\hat{L}} - V_{\hat{L}}\left(\frac{\partial p^*}{\partial y}\right)_{\hat{L}} + \frac{\rho V_{\hat{L}}}{\Delta t}v^n \tag{4.5}$$

Now, the correct pressure field p is obtained as:

$$p^{n+1}_{\hat{L}} = p^*_{\hat{L}} + p^{'}_{\hat{L}} \tag{4.6}$$

in which $p^{'}$ is the pressure correction term. Subsequently, we need to investigate how the velocity components respond to this change in pressure. In that fashion, we can introduce the corresponding velocity corrections $u^{'}$ and $v^{'}$ as:

$$u^{n+1}_{\hat{L}} = u^*_{\hat{L}} + u^{'}_{\hat{L}} \tag{4.7}$$

$$v^{n+1}_{\hat{L}} = v^*_{\hat{L}} + v^{'}_{\hat{L}} \tag{4.8}$$

Subtracting Equation 4.2 (resp. 4.3) from Equation 4.4 (resp. 4.5) we get:

$$a_{u,\hat{L}}(u^{n+1}_{\hat{L}} - u^*_{\hat{L}}) = \sum_{i=1}^{nb}(a_{u,nb}(u^{n+1}_{nb} - u^*_{nb}))_{\hat{L}} - V_{\hat{L}}\left(\frac{\partial(p^{n+1} - p^*)}{\partial x}\right)_{\hat{L}} \tag{4.9}$$

$$a_{v,\hat{L}}(v^{n+1}_{\hat{L}} - v^*_{\hat{L}}) = \sum_{i=1}^{nb}(a_{v,nb}(v^{n+1}_{nb} - v^*_{nb}))_{\hat{L}} - V_{\hat{L}}\left(\frac{\partial(p^{n+1} - p^*)}{\partial y}\right)_{\hat{L}} \tag{4.10}$$

Substituting Equation 4.6 and Equation 4.7 (resp. 4.8) in Equation 4.9 (resp. 4.10):

$$a_{u,\hat{L}}u^{'}_{\hat{L}} = \sum_{i=1}^{nb}(a_{u,nb}u^{'}_{nb})_{\hat{L}} - V_{\hat{L}}\left(\frac{\partial p^{'}}{\partial x}\right)_{\hat{L}} \tag{4.11}$$

$$a_{v,\hat{L}}v^{'}_{\hat{L}} = \sum_{i=1}^{nb}(a_{v,nb}v^{'}_{nb})_{\hat{L}} - V_{\hat{L}}\left(\frac{\partial p^{'}}{\partial y}\right)_{\hat{L}} \tag{4.12}$$

The SIMPLEC algorithm proposes that the term related to the neighbours velocity correction should be approximate as follows:

$$\sum_{i=1}^{nb}(a_{v,nb}u^{'}_{nb})_{\hat{L}} \approx \sum_{i=1}^{nb}(a_{v,nb}u^{'}_{\hat{L}})_{\hat{L}} \tag{4.13}$$

$$\sum_{i=1}^{nb}(a_{v,nb}v^{'}_{nb})_{\hat{L}} \approx \sum_{i=1}^{nb}(a_{v,nb}v^{'}_{\hat{L}})_{\hat{L}} \tag{4.14}$$

We can rewrite Equation 4.11 and Equation 4.12 as:

$$\left(a_{u,\hat{L}} - \sum_{i=1}^{nb}(a_{u,nb})\right) u_{\hat{L}}^{'} = -V_{\hat{L}} \left(\frac{\partial p^{'}}{\partial x}\right)_{\hat{L}} \tag{4.15}$$

$$\left(a_{v,\hat{L}} - \sum_{i=1}^{nb}(a_{v,nb})\right) u_{\hat{L}}^{'} = -V_{\hat{L}} \left(\frac{\partial p^{'}}{\partial y}\right)_{\hat{L}} \tag{4.16}$$

that can be rewrite as follows:

$$u_{\hat{L}}^{'} = d_{u,\hat{L}} \left(\frac{\partial p^{'}}{\partial x}\right)_{\hat{L}} \tag{4.17}$$

$$u_{\hat{L}}^{'} = d_{v,\hat{L}} \left(\frac{\partial p^{'}}{\partial y}\right)_{\hat{L}} \tag{4.18}$$

in which:

$$d_{v,\hat{L}} = -\frac{V_{\hat{L}}}{\left(a_{u,\hat{L}} - \sum_{i=1}^{nb}(a_{u,nb})\right)} \tag{4.19}$$

$$d_{v,\hat{L}} = -\frac{V_{\hat{L}}}{\left(a_{v,\hat{L}} - \sum_{i=1}^{nb}(a_{v,nb})\right)} \tag{4.20}$$

Then, the velocity correction equations, Equation 4.7 and Equation 4.8, can be written in terms of the pressure correction as:

$$u_{\hat{L}}^{n+1} = u_{\hat{L}}^{*} + d_{u,\hat{L}} \left(\frac{\partial p^{'}}{\partial x}\right)_{\hat{L}} \tag{4.21}$$

$$v_{\hat{L}}^{n+1} = v_{\hat{L}}^{*} + d_{v,\hat{L}} \left(\frac{\partial p^{'}}{\partial y}\right)_{\hat{L}} \tag{4.22}$$

Up to this point, we only considered the conservation of momentum equation, but as mentioned before, the velocity field must satisfy the divergence-free condition. As mentioned in Section 3.2.6.1, we can estimate the fluid velocity in the surface of a generic control volume $\hat{L}$ by means of a momentum a momentum interpolation scheme. By following this procedure, it is possible to obtain a pressure correction equation as:

$$\sum_{\Gamma_{IJ} \in \Gamma_{\hat{L}}} (\mathbf{u}_{IJ} \mathbf{n}_{IJ} \|IJ\|) = 0 \tag{4.23}$$

In order to estimate the cell face velocities, for each component u and v, we will follow the same procedure described in 3.2.6.1. In that fashion, the cell face velocities can be written as:

$$u_e = \overline{u_e^*} + \frac{d_{u,\hat{L}}}{2} \left(\frac{\partial p^{'}}{\partial x}\right)_{\hat{L}} + \frac{d_{u,\hat{R}}}{2} \left(\frac{\partial p^{'}}{\partial x}\right)_{\hat{R}} - d_{u,e} \left(\frac{\partial p^{'}}{\partial x}\right)_{e} + \frac{\rho_e V_e}{a_{u,e}\, \Delta t} u_e^n \tag{4.24}$$

$$v_e = \overline{v_e^*} + \frac{d_{v,\hat{L}}}{2}\left(\frac{\partial p^{'}}{\partial y}\right)_{\hat{L}} + \frac{d_{v,\hat{R}}}{2}\left(\frac{\partial p^{'}}{\partial y}\right)_{\hat{R}} - d_{v,e}\left(\frac{\partial p^{'}}{\partial y}\right)_{e} + \frac{\rho_e V_e}{a_{v,e}\,\Delta t} v_e^n \tag{4.25}$$

in which:

$$\overline{u_e^*} = \frac{u_{\hat{L}}^* + u_{\hat{R}}^*}{2} \tag{4.26}$$

$$\overline{v_e^*} = \frac{v_{\hat{L}}^* + v_{\hat{R}}^*}{2} \tag{4.27}$$

and the transient term, u_e^n and v_e^n , can be approximated using Equation 3.53.

After solving Equation 4.23 we get a pressure correction field, $p^{'}$, for all control volumes, that will be used to update the velocity and the pressure fields as:

$$p_{\hat{L}}^{n+1} = p_{\hat{L}}^* + p_{\hat{L}}^{'} \tag{4.28}$$

$$u_{\hat{L}}^{n+1} = u_{\hat{L}}^* + d_{u,\hat{L}}\left(\frac{\partial p^{'}}{\partial x}\right)_{\hat{L}} \tag{4.29}$$

$$v_{\hat{L}}^{n+1} = v_{\hat{L}}^* + d_{v,\hat{L}}\left(\frac{\partial p^{'}}{\partial y}\right)_{\hat{L}} \tag{4.30}$$

The complete SIMPLEC algorithm procedure can be seen on Figure 9. It is important to notice that in order to update the velocity field, u^* and v^*, for the next time step, it must satisfy both, the momentum equation and the divergence-free condition (Condition 1).

Figure 9 – SIMPLEC Flowchart.

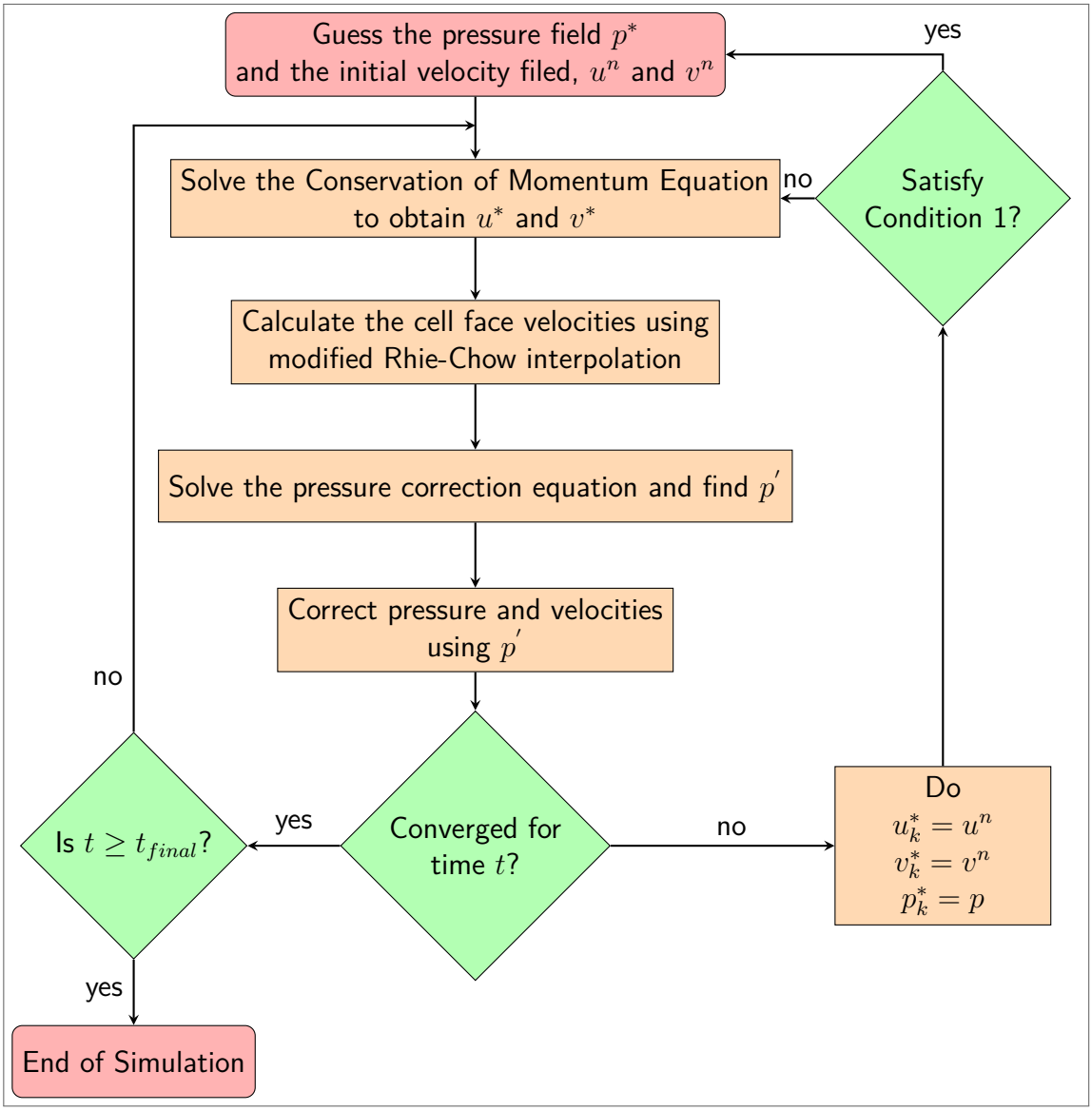

Source: Author.

5 NUMERICAL RESULTS

In this section, we present four examples in order to evaluate the accuracy and robustness of our numerical formulation. In the first one, we simulate a steady state flow through a channel filled with porous material for which there is an analytical solution. The second example consists in a transient flow in a channelized carbonate (karst) domain. In the third one, we evaluate the robustness of our formulation to model the one phase flow in a quarter of five-spot configuration with four vuggy structures with a high contrast in permeability when compared with the porous material. In the final example, we consider a $1/4$ five-spot with vuggy structures connected by a network of fractures.

In order to compare the the numerical results, initially we define the L2-norm of the error Eq. 5.1, and the convergence rate Eq. 5.2.

$$\varepsilon_{L_2} = \left(\frac{\sum_{\hat{L}\in\Omega}(v_{analytical}(x_{\hat{i}}) - v_{numerical}(x_{\hat{i}}))}{\sum_{\hat{L}\in\Omega}(v_{analytical}(x_{\hat{i}}))} \right)^{\frac{1}{2}} \tag{5.1}$$

$$q = \log_2 \left(\frac{\varepsilon_i}{\varepsilon_{i+1}} \right) \tag{5.2}$$

5.1 STEADY STATE FLOW THROUGH A CHANNEL FILLED WITH POROUS MATERIAL

This problem was adapted from (JHA; KAURANGINI, 2011) in order to study fully developed and laminar fluid flow in a channel defined by two parallel plates with a distance H between them, see Figure 10. The channel is filled with isotropic porous material with permeability given by $\mathbf{K} = k\mathbf{I}$. The fluid is considered incompressible, and the dynamic and effective viscosities are equal, i.e. $\mu' = \mu$. For this problem, the athors proposed a analytical solution for the Brinkman-Forchheimer-Extended-Darcy flow model, defined as:

$$\frac{\mu}{\mu'}\frac{d^2v}{dy^2} - \frac{H^2}{k}v - \frac{C}{\sqrt[4]{\left(\frac{k}{H^2}\right)^n}}v^n - \frac{H^3}{\rho v^2}\frac{dp}{dx} = 0 \tag{5.3}$$

in which the C is the coefficient of inertia.

We also neglect the third term in the left hand side of Equation 5.3, known as Forchheimer's term, by adopting a Reynolds number smaller than 1, consequently the analytical solution of Equation 5.3 is given by (JHA; KAURANGINI, 2011):

Figure 10 – Representation of the physical and geometric parameters for the Steady State Flow Through a Channel Filled with Porous Material.

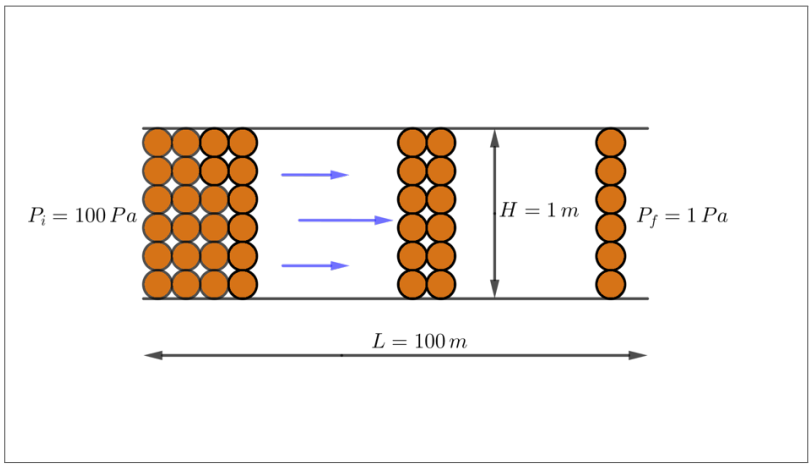

Source: Author.

$$v(y) = \frac{\sinh(\lambda(1-y))}{\sinh(y)} - \frac{G}{\lambda^2\gamma}\left(\frac{\sinh(\lambda(1-y)) + \sinh(\lambda y)}{\sinh(y)}\right) \tag{5.4}$$

where G is the dimensionless pressure gradient imposed along the channel in the x direction, defined as:

$$G = -\frac{H^3}{\rho\mu^2}\frac{\Delta p}{L} \tag{5.5}$$

and γ is the ratio between the effective and dynamic viscosities, and λ is given by:

$$\lambda = \frac{1}{\sqrt{\gamma}}\sqrt{\left(\frac{H^2}{k} + \frac{1}{\sqrt[4]{\frac{k}{H^2}}}\right)} \tag{5.6}$$

By making these assumptions it was possible to compare the numerical results of the proposed scheme with the analytical solution provided by Equation 5.4. In order to do so, a pressure drop, G, of $99psi$ was imposed along the x direction, and no-flow boundary conditions were imposed on the upper and lower boundaries, the channel height H=1,0 m and the length of the domain is L=100m. For this problem, we have adopted a uniform quadrilateral structured mesh of 128 $\times$ 128 control volumes and different values of permeability, $k = 1.5 \times 10^{-15}\,m^2$, $k = 1.5 \times 10^{-13}\,m^2$, $k = 1.5 \times 10^{-12}\,m^2$, were tested in order to simulate the different fluid flow regions that exist on carbonate reservoirs.

Figure 11 – Steady State Flow Through a Channel Filled with Porous Material: Computational mesh with 128 control volumes in vertical direction and the fluid velocity profiles through the center line for the problem of the flow through a channel filled with porous material for a value of the permeability equal to a) $k = 1.5 \times 10^{-15}\, m^2$; b) $k = 1.5 \times 10^{-13}\, m^2$; c) $k = 1.5 \times 10^{-12}\, m^2$.

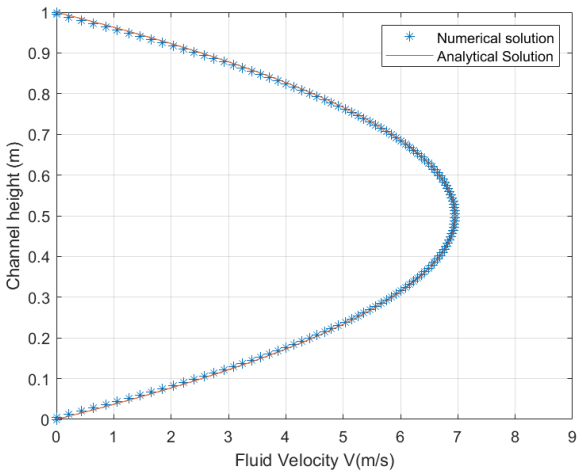

(a)

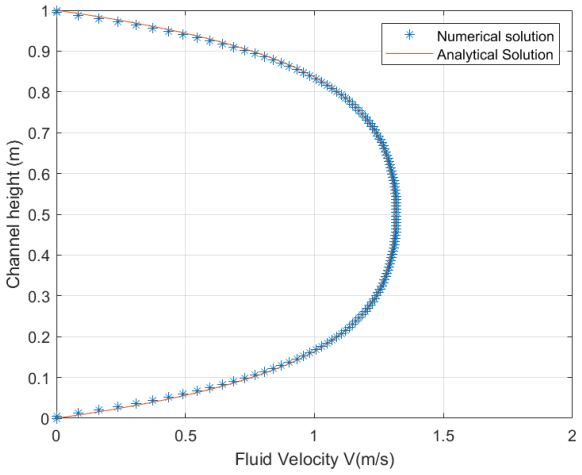

(b)

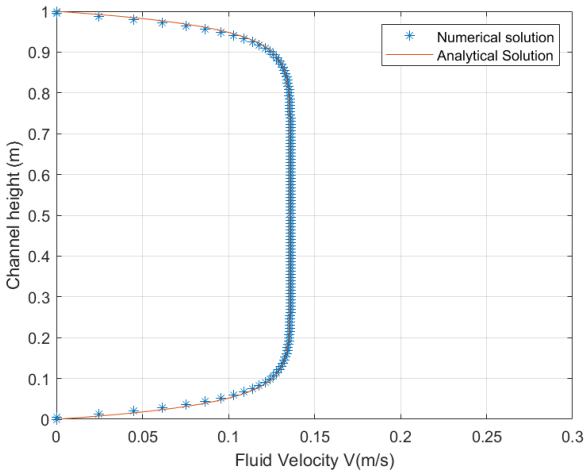

(c)

Source: Author.

By analysing the Figure 11, it can be clearly seen that when the value of the permeability increases, the velocity profile becomes essentially parabolic as it is expected in the free flow region. In all cases, we can notice the excellent agreement between the analytical and the numerical solutions obtained using our formulation.

In order to evaluate the convergence rate of our scheme, we evaluate the behavior of the L2 norm of the error for the velocity field for different mesh densities with the mesh spacing as shown in Table 1 .As expected, the error has a decreasing behavior during the mesh refinement Figure 12.

Table 1 – Errors and convergence rates for different values of permeability

	$k = 1.5 \times 10^{-12}\, m^2$		$k = 1.5 \times 10^{-14}\, m^2$		$k = 1.5 \times 10^{-15}\, m^2$	
Vertical CVs	ε_{L_2}	q	ε_{L_2}	q	ε_{L_2}	q
8	3.18×10^{-3}	-	8.91×10^{-3}	-	1.86×10^{-3}	-
16	9.14×10^{-4}	1.798	2.73×10^{-3}	1.704	5.49×10^{-4}	1.761
32	2.69×10^{-4}	1.764	8.31×10^{-4}	1.748	1.52×10^{-4}	1.856
64	7.29×10^{-5}	1.833	2.43×10^{-4}	1.742	4.33×10^{-5}	1.806
128	2.19×10^{-6}	1.833	6.78×10^{-5}	1.841	1.27×10^{-5}	1.766

Source: Author.

Figure 12 – Steady State Flow Through a Channel Filled with Porous Material: Error behavior related to the mesh refinement, using a permeability of $k = 1.5 \cdot 10^{-15} m^2$, $k = 1.5 \cdot 10^{-14} m^2$ and $k = 1.5 \cdot 10^{-13} m^2$.

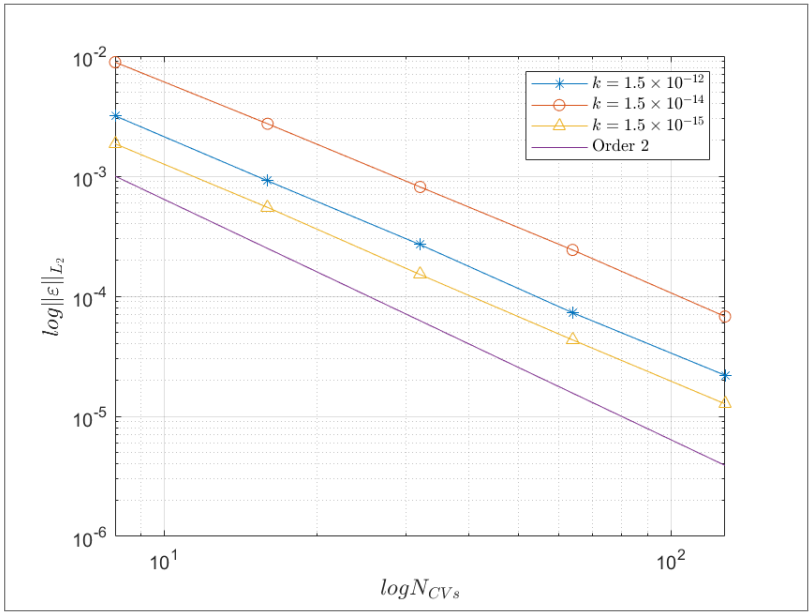

Source: Author.

5.2 TRANSIENT FLOW IN A CHANNELIZED CARBONATE KARST DOMAIN

In this example, adapted from (BI et al., 2009), we consider a square $[1 \times 1]$ porous domain which contains a vuggy structure represented by a circle, with a radius of 0.25m positioned at the center of the domain. A pressure drop of 1 psi was imposed along the x direction, and no-flow boundary conditions were imposed on the upper and bottom boundaries of the reservoir. The domain was discretized using a triangular mesh, see Figure 13. The rock matrix is considered homogeneous and isotropic with permeability tensor given by $\mathbf{K} = k\mathbf{I}$ with $k = 1.5 \times 10^{-15}\, m^2$, and the in the vugs regions, $k = 1.5 \times 10^{-12}\, m^2$. The pressure distribution presented in Figure 14 shows the effects of the vugs on the pressure distribution, moreover in Figure 15 shows that at the close to the vugs the velocity field pattern are changed significantly.

Figure 13 – Transient Flow in a Channelized Carbonate Karst Domain: Geometry, mesh and wells, or the problem of the transient flow in a channelized carbonate (karst) domain.

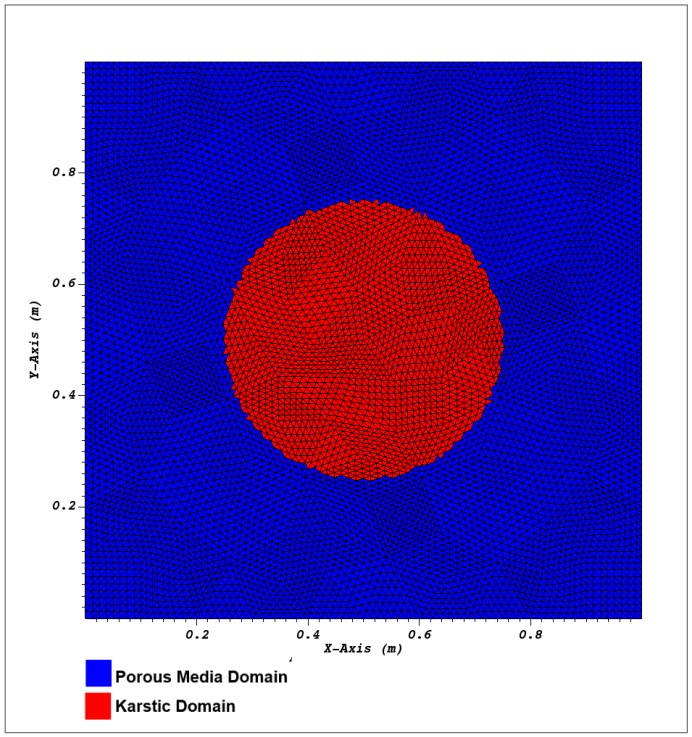

Source: Author.

Figure 14 – Transient Flow in a Channelized Carbonate Karst Domain:Pressure distribution for the problem of the transient flow in a channelized carbonate (karst) domain using an unstructured mesh with 15,488 triangular control volumes at t=100 days.

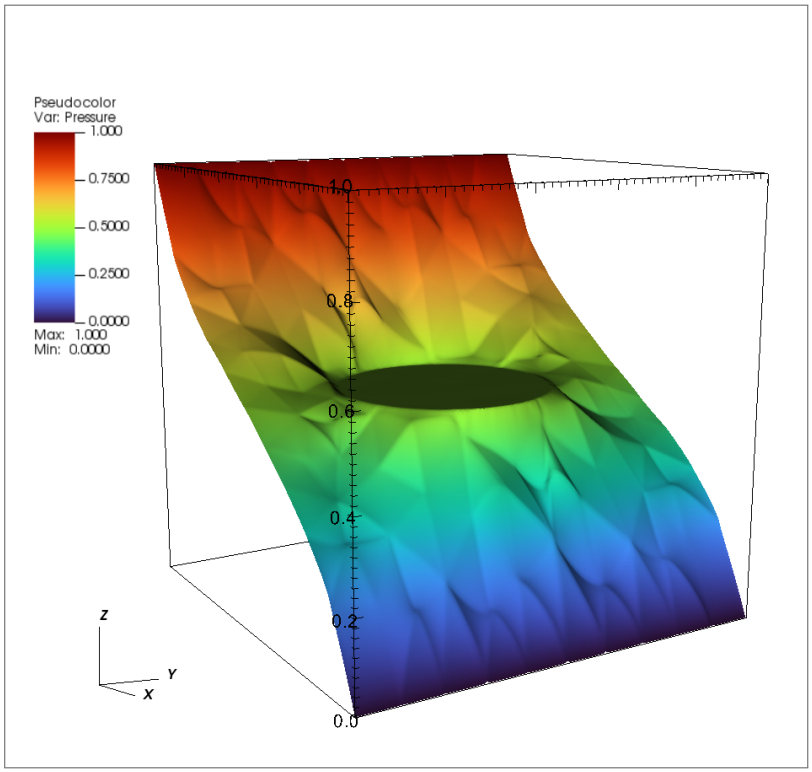

Source: Author.

Figure 15 – Transient Flow in a Channelized Carbonate Karst Domain:Pressure distribution for the problem of the transient flow in a channelized carbonate (karst) domain using an unstructured mesh with 15,488 triangular control volumes at t=100 days.

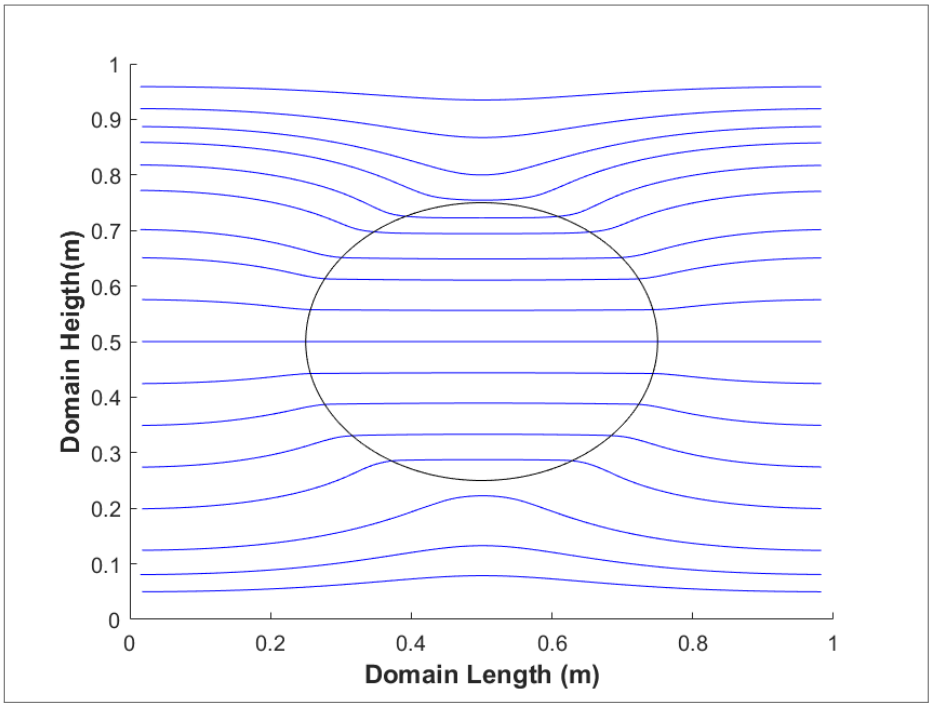

Source: Author.

In Figure 16 we present the solutions obtained on a sequence of sucessively refined triangular meshes with 242, 968, 3,872, 15,488 and compared the behavior of the pressure field to the reference solution obtained with 61,952 control volumes.

Figure 16 – Transient Flow in a Channelized Carbonate Karst Domain: Pressure drop along the diagonal connecting the bottom left part (x=0;y=1) to the upper right part (x=1;y=0) of the reservoir for the problem of the transient flow in a channelized carbonate (karst) domain with different sucessively refined unstructured triangular meshes with 242; 968; 3,872; 15,488 and 61,952 control volumes.

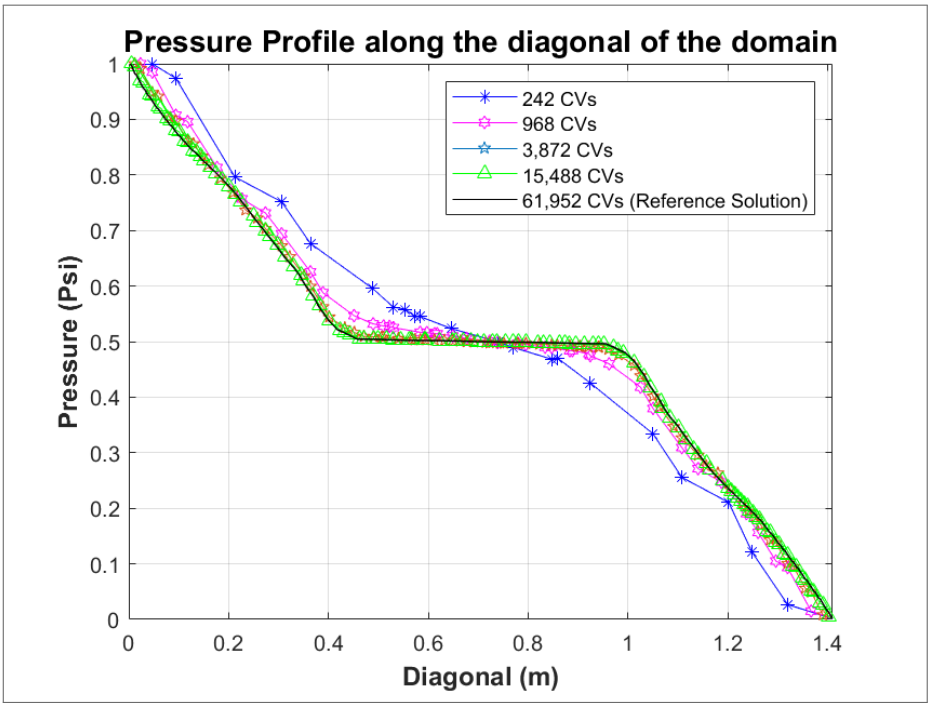

Source: Author.

In order to verify the segregated approach, for the same problem, the errors and the numerical convergence rates for both, the monolithic and the segregated approaches are presented in Table 2 , considering triangular meshes with 242, 968 and 3,872 control volumes. In Figure 17 we present the pressure drop along the diagonal connecting the bottom left part to the upper right part of the reservoir using the monolithic and the SIMPLEC approaches with a triangular mesh with 3,872 control volumes alongside the reference pressure that was considered using a monolithic approach with 15,488 triangular control volumes.

Table 2 – Transient Flow in a Channelized Carbonate Karst Domain: Errors and convergence rates for the monolithic and the SIMPLEC approaches

# CVs		242	968	3,872
SIMPLEC	ε_{L_2}	1.487×10^{-2}	4.109×10^{-3}	1.193×10^{-3}
	q	-	1.855	1.783
Monolithic	ε_{L_2}	1.321×10^{-2}	3.499×10^{-3}	9.794×10^{-4}
	q	-	1.916	1.837

Source: Author.

Figure 17 – Transient Flow in a Channelized Carbonate Karst Domain: Pressure drop along the diagonal connecting the bottom left part to the upper right part of the reservoir for the triangular mesh with 3,872 control volumes using the monolith and the SIMPLEC approaches.

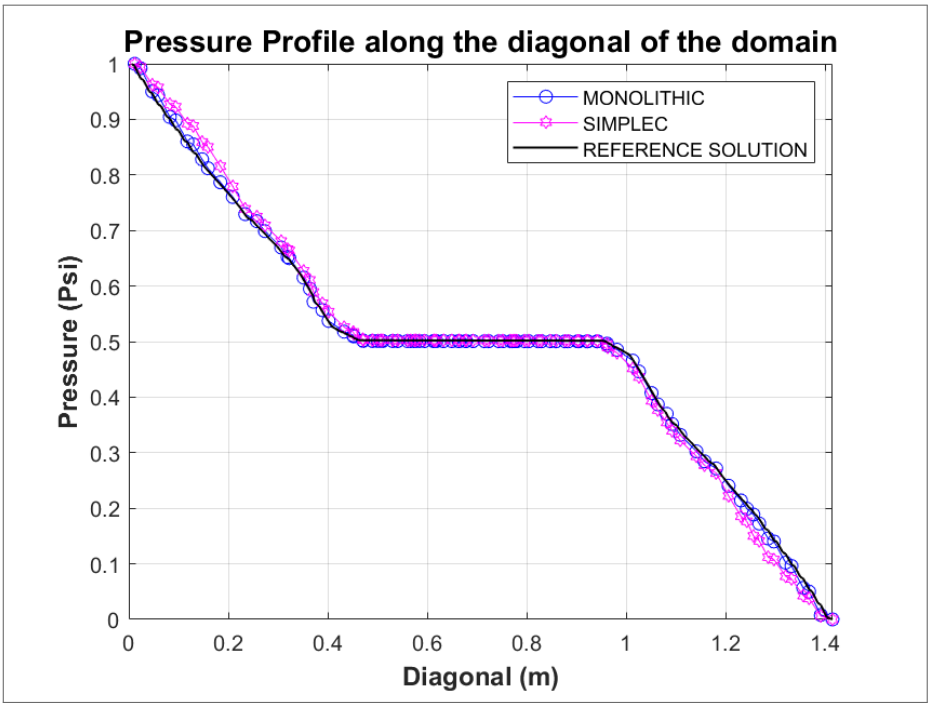

Source: Author.

By analysing the results obtained in Figures. 13, 16 and 17 it is possible to infer that our formulation, using both approaches, is capable to model the fluid flow in the porous media (Darcy flow) and in the vugular free flow region (Stokes flow). It worth mentioning that our results compare quite well with those presented in (BI et al., 2009).

5.3 ONE PHASE FLOW IN A POROUS DOMAIN WITH FOUR VUGGY STRUCTURES WITH A 1/4 OF FIVE-SPOT CONFIGURATION

This example consists in square $[1 \times 1]$ porous domain with four elliptical vuggy structures within it, as shown in Figure 19.

In this problem, we will evaluate three different scenarios: 1. a strictly Darcy flow; 2. the permeability of the vugs has a value that represents a free flow region; 3. the permeability tensor is rotated in the rock matrix to appraise our scheme for full tensor permeability. This model provides verification of the proposed scheme by adopting three different case studies: first an homogeneous porous media to test the scheme in a Darcy fluid flow configuration, subsequently the permeability of the vugs will be changed to a value that can represent a free flow region inside those geological features, and finally we will perform a rotation on the permeability tensor in the matrix region in order to test the proposed scheme with full tensors.

Figure 18 – One phase flow in a porous domain with four vuggy structures with a 1/4 of five-spot configuration: Geometry, mesh and wells, for the one phase flow in a porous domain with four vuggy structures with a 1/4 of five-spot configuration.

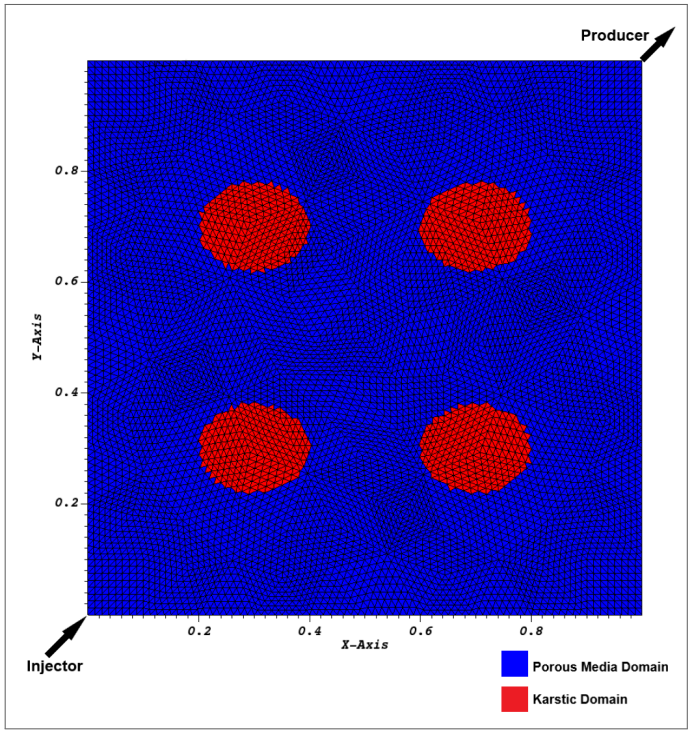

Source: Author.

5.3.1 Homogeneous Porous Media

In the first case, we consider a homogeneous and isotropic permeability tensor for the whole reservoir including the four elliptic regions, with K=kI and $k = 1.5 \times 10^{-}15\, m^2$. The fluid viscosity is $\mu = 0.7$ cP. Pressure at the injection well is $p_i = 1$ psi and $p_p = 0$ at the producer well. In Figure **??**, we present the pressure field, which, as expected reproduces quite well the expected solution profile for this $1/4$ of five-spot problem.

Figure 19 – Homogeneous Porous Media: Pressure distribution along the domain on a homogeneous Porous Media in t=100 days.

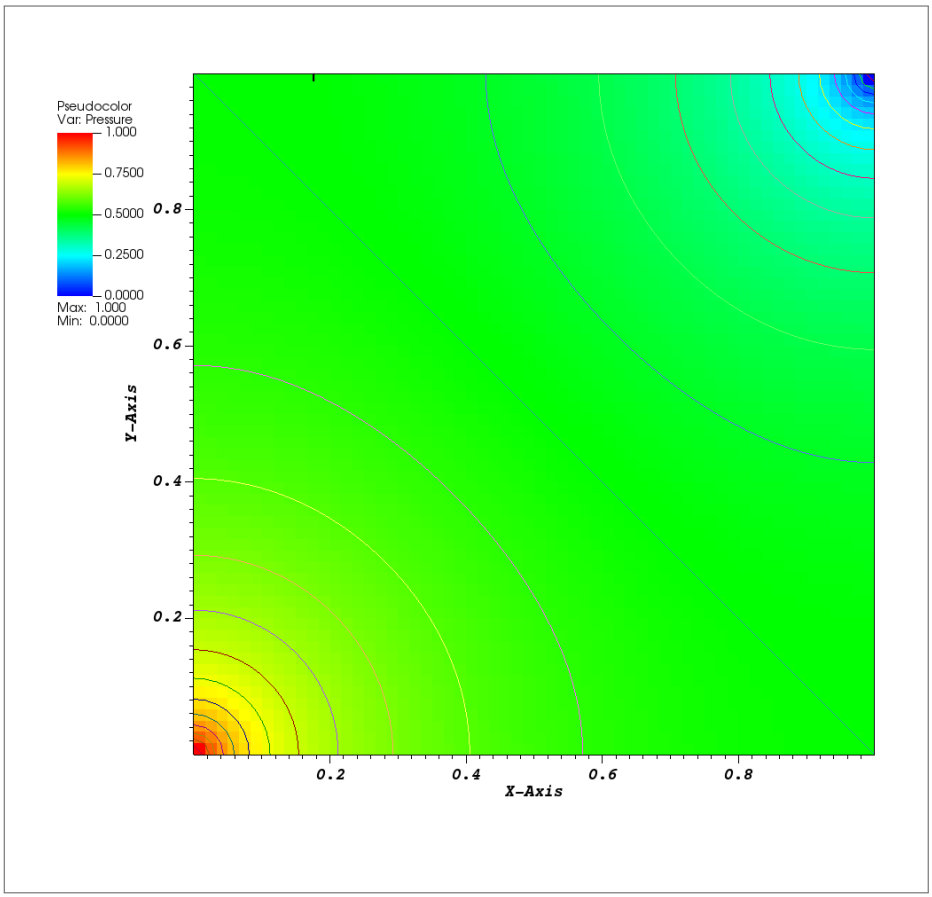

Source: Author.

5.3.2 Heterogeneous and Isotropic Porous Media

In the second case, in order to verify the influence of the vuggy structures on the fluid flow pattern, we considered a isotropic rock permeability tensor, $\mathbf{K} = k\mathbf{I}$, with $k = 1.5 \times 10^{-12}\, m^2$, in the vuggy regions, and $k = 1.5 \times 10^{-15}\, m^2$ in the rock matrix. As in the previous case, the fluid viscosity is $\mu = 0.7$ cP. Pressure at the injection well is $p_i = 1$ psi and $p_p = 0$ psi at the

producer well.

The pressure distribution presented in Figures 20, 21 and 22, in different time steps, shows that the presence of the karstic formations alter significantly the pressure distributions, specially at the regions of the domain near the structures. Furthermore, the fluid flow streamlines, Figure 23, at $t = 100$ days, are diverted due the presence of the regions with high permeabilities.

Figure 20 – Heterogeneous and Isotropic Porous Media: Pressure distribution for the heterogeneous reservoir with four vuggy regions in a $1/4$ of five-spot configuration using an unstructured mesh with 3,872 triangular control volumes, in $t = 1$ day.

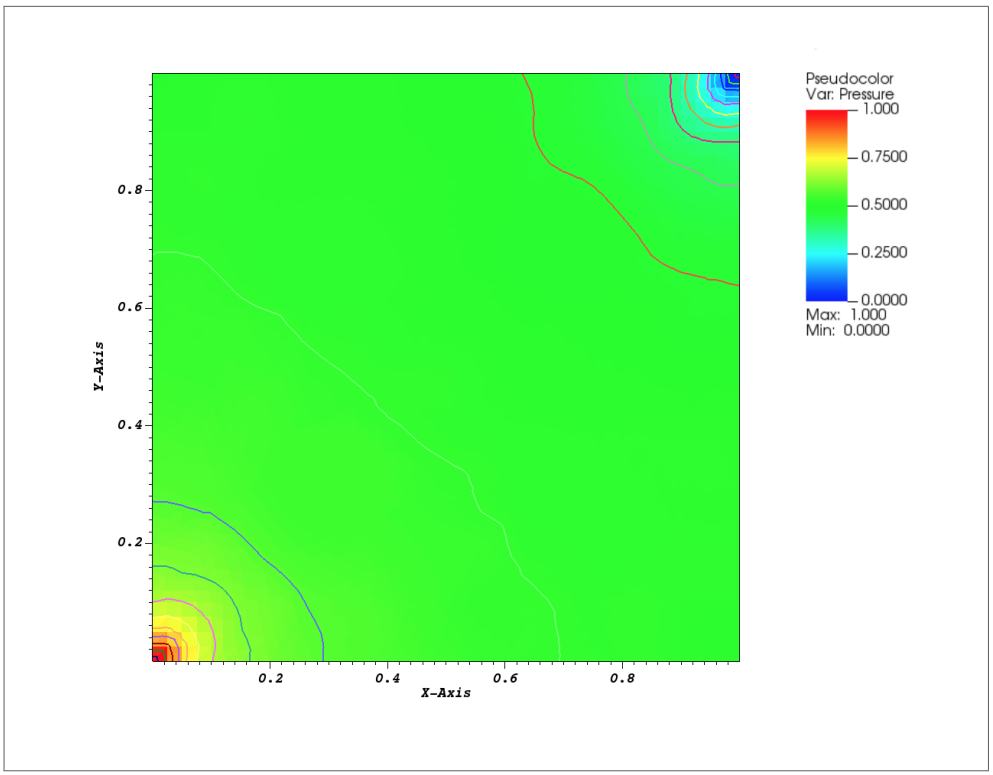

Source: Author.

Figure 21 – Heterogeneous and Isotropic Porous Media: Pressure distribution for the heterogeneous reservoir with four vuggy regions in a $1/4$ of five-spot configuration using an unstructured mesh with 3,872 triangular control volumes, in $t = 10$ days.

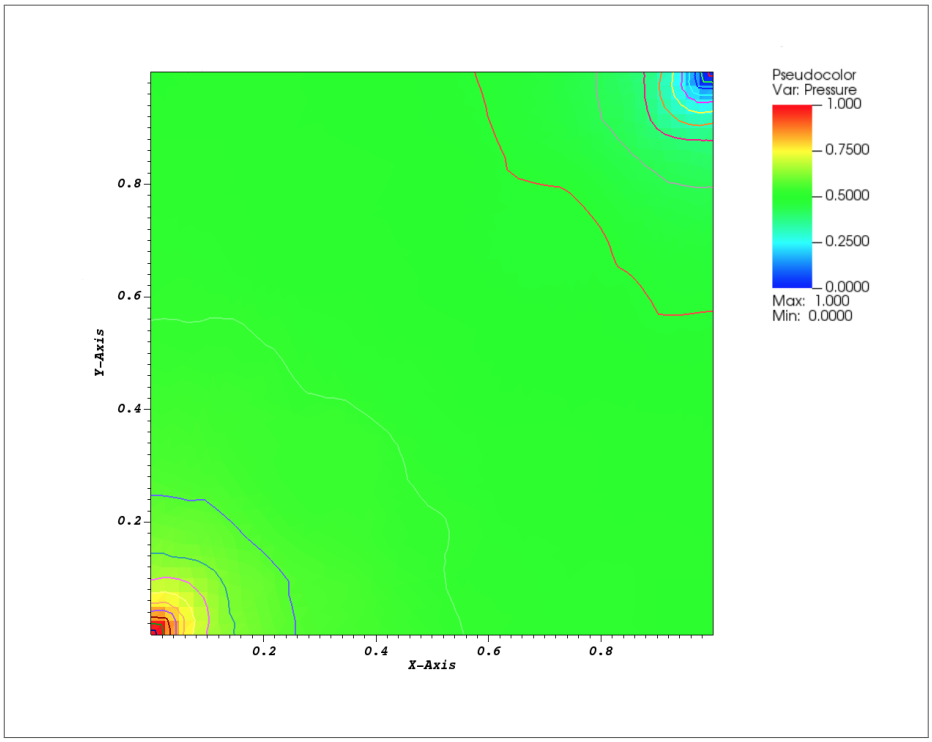

Source: Author.

Figure 22 – Heterogeneous and Isotropic Porous Media: Pressure distribution for the heterogeneous reservoir with four vuggy regions in a $1/4$ of five-spot configuration using an unstructured mesh with 3,872 triangular control volumes, in $t = 100$ days.

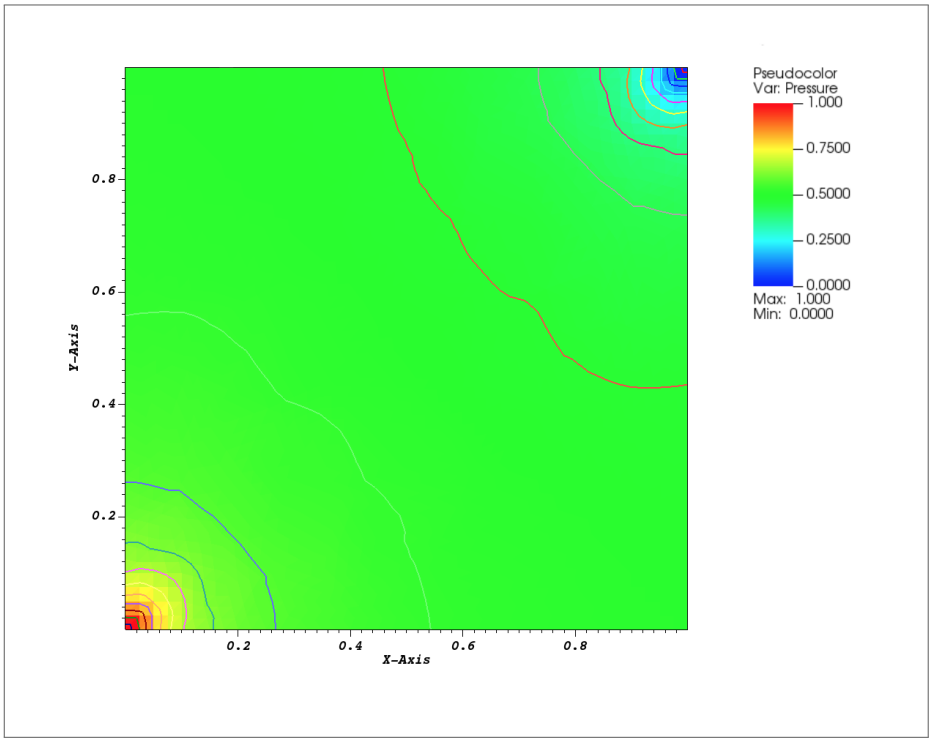

Source: Author.

Figure 23 – Heterogeneous and Isotropic Porous Media: Streamlines, at $t = 100$ days, along the domain on a Heterogeneous Isotropic Porous Media with karstification.

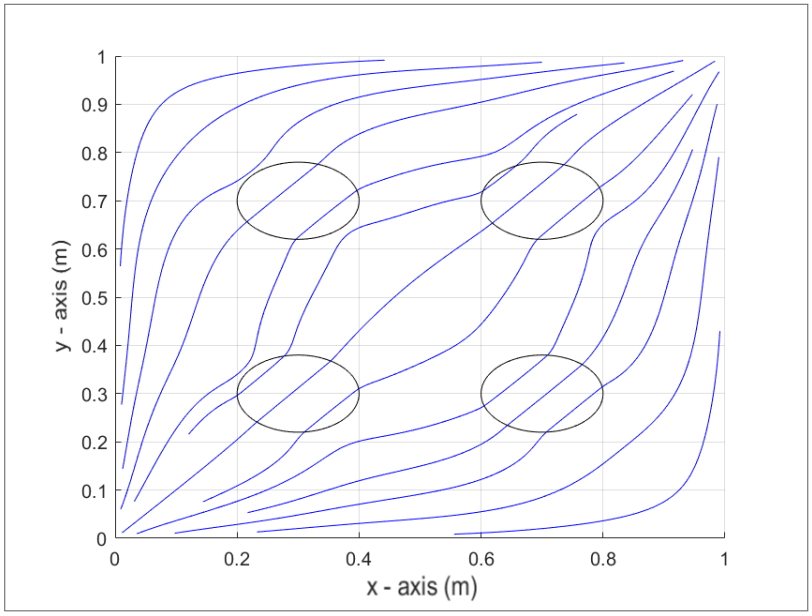

Source: Author.

In Figure 24, we present the pressure field obtained along the diagonal connecting the injection and the production wells, with different mesh densities, with 242; 968; 3,872 and 15,872 control volumes and the reference solution obtained for the mesh with 61,952 control volumes.

Figure 24 – Heterogeneous and Isotropic Porous Media: Pressure drop along the diagonal connecting the injection and the producer wells for the heterogeneous reservoir with four vuggy regions in a 1/4 of five-spot configuration for different triangular mesh densities with 242; 968; 3,872; 15,488 control volumes and the reference solution obtained with 61,952 control volumes.

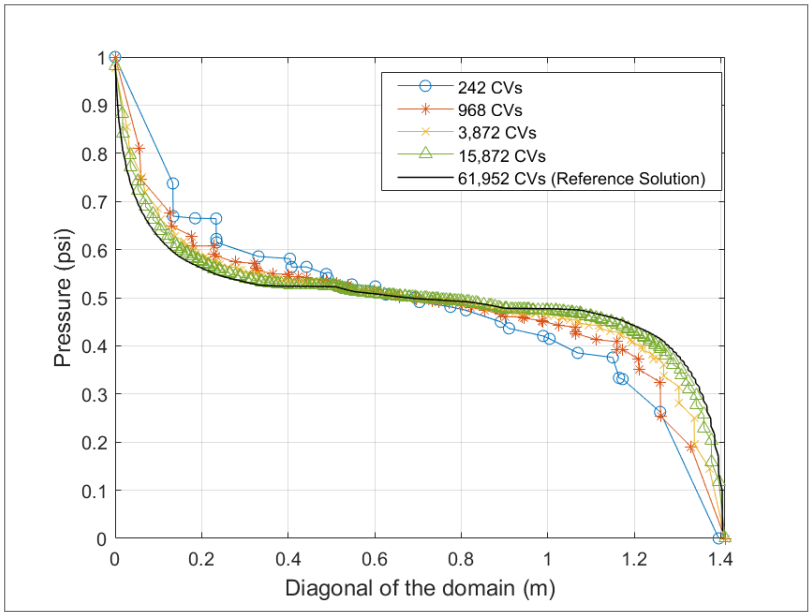

Source: Author.

Additionally, with the aim to verify the segregated approach, for the problem of a Heterogeneous and Isotropic Porous Media, the errors and the numerical convergence rates for both, the monolithic and the segregated approaches are presented in Table 3 , considering triangular meshes with 242, 968 and 3,872 control volumes. In Figure 25 we present the pressure drop along the diagonal connecting the bottom left part to the upper right part of the reservoir using the monolithic and the SIMPLEC approaches with a triangular mesh with 3,872 control volumes alongside the reference pressure that was considered using a monolithic approach with 15,488 triangular control volumes.

Table 3 – Heterogeneous and Isotropic Porous Media: Errors and convergence rates for the monolithic and the SIMPLEC approaches

# CVs		242	968	3,872
SIMPLEC	ε_{L_2}	9.631×10^{-2}	2.855×10^{-2}	8.693×10^{-3}
	q	-	1.754	1.716
Monolithic	ε_{L_2}	9.38×10^{-2}	2.591×10^{-3}	7.121×10^{-4}
	q	-	1.856	1.863

Source: Author.

Figure 25 – Heterogeneous and Isotropic Porous Media: Pressure drop along the diagonal connecting the bottom left part to the upper right part of the reservoir for the triangular mesh with 3,872 control volumes using the monolith and the SIMPLEC approaches.

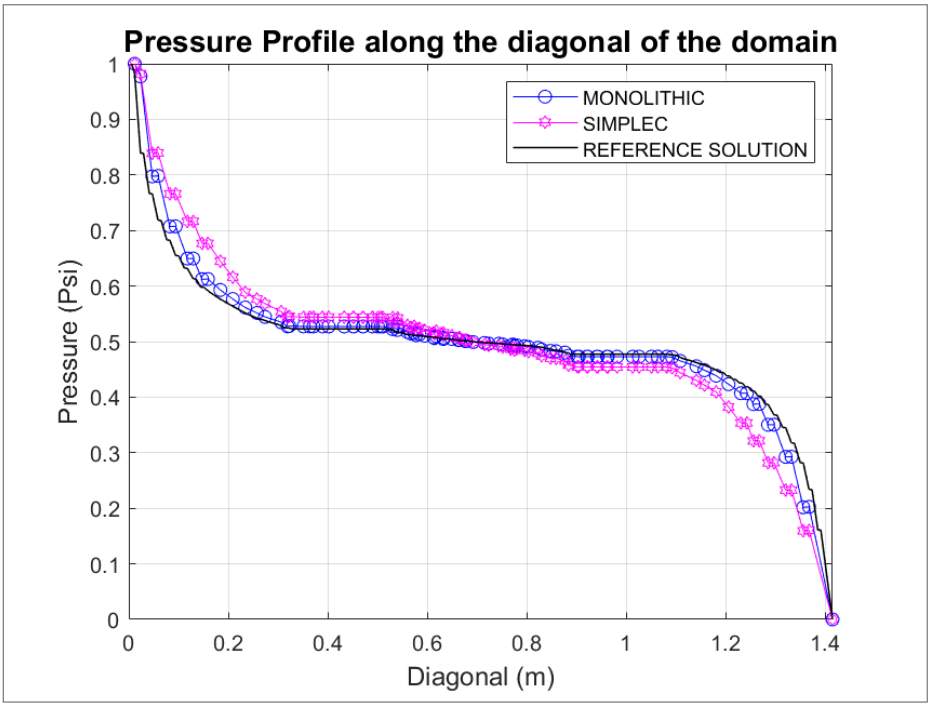

Source: Author.

By analysing the results in this case study scenario, it is possible to infer that the proposed scheme, by adopting the monolithic and segregated approaches, is able to capture the phenomena on the karstic structures on carbonate reservoirs.

5.3.3 Heterogeneous and Anisotropic Reservoir with Four Vuggy Regions in a 1/4 of Five-Spot Configuration

In this third case, we consider the one-phase flow in a heterogeneous and anisotropic reservoir with four vuggy regions. In the rock matrix the permeability is a full tensor given by Equation 5.8 and Equation 5.7. The permeability inside the vugs is given by $\mathbf{K} = k\mathbf{I}$ with $k = 1.5 \times 10^{-12}\, m^2$. We have used an unstructured triangular mesh with 3,872 control volumes. The rock permeability tensor in the rock matrix is defined as

$$\mathbf{K} = \mathcal{R} \begin{bmatrix} 1.5 \cdot 10^{-14} & 0 \\ 0 & 1.5 \cdot 10^{-15} \end{bmatrix} \mathcal{R}^{\top} \tag{5.7}$$

The anticlockwise, rotation matrix, $\mathcal{R}$, is defined as:

$$\mathcal{R} = \begin{bmatrix} \cos\theta & \sin\theta \\ -\sin\theta & \cos\theta \end{bmatrix}, \quad \text{with} \quad \theta = \frac{\pi}{6} \tag{5.8}$$

The pressure distribution seen on Fig 26, by comparing with the Figure **??** (c), at $t = 100$ days, we can infer that the anisotropy of the rock matrix regions alter pronouncedly the pressure distribution. Moreover, the fluid flow streamlines, Figure 27 are distorted when compared with the previous case due the anisotropy of the rock matrix.

Figure 26 – Heterogeneous and anisotropic reservoir with four vuggy regions in a 1/4 of five-spot configuration: Pressure Distribution along the domain on a Heterogeneous Anisotropic Porous Media with 3,872 triangular control volumes.

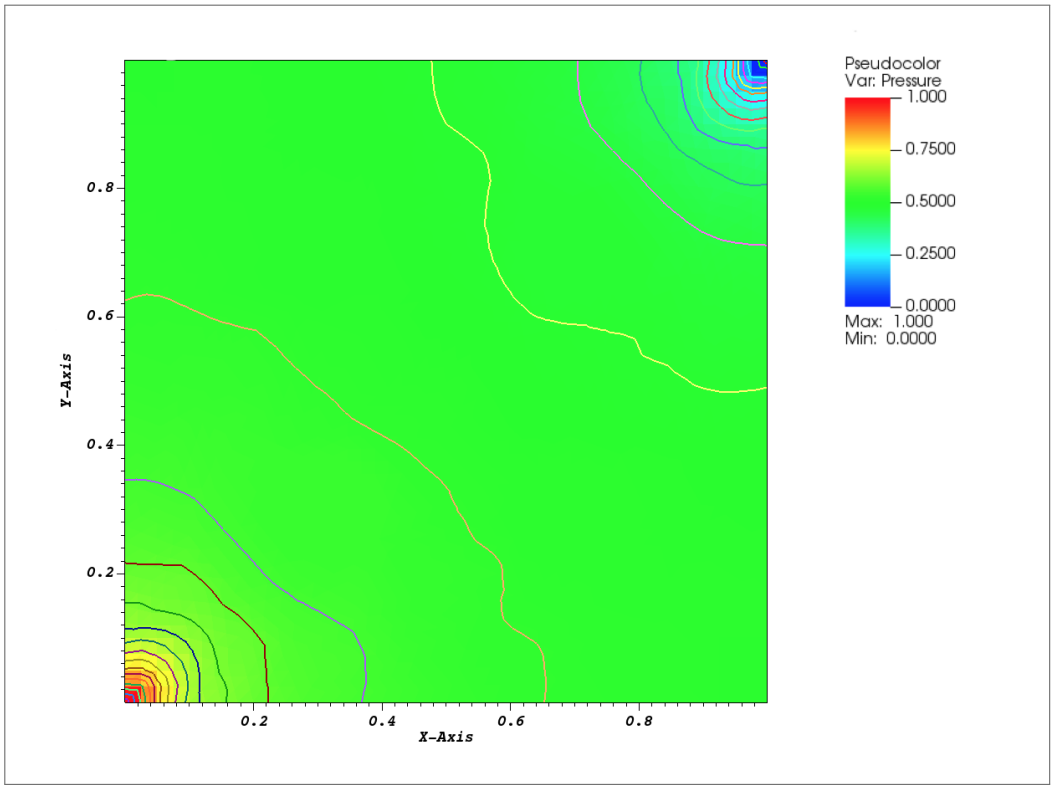

Source: Author.

Figure 27 – Heterogeneous and Anisotropic Reservoir with Four Vuggy Regions in a 1/4 of Five-Spot Configuration: Streamlines a Heterogeneous Anisotropic Porous Media with 3,872 triangular control volumes.

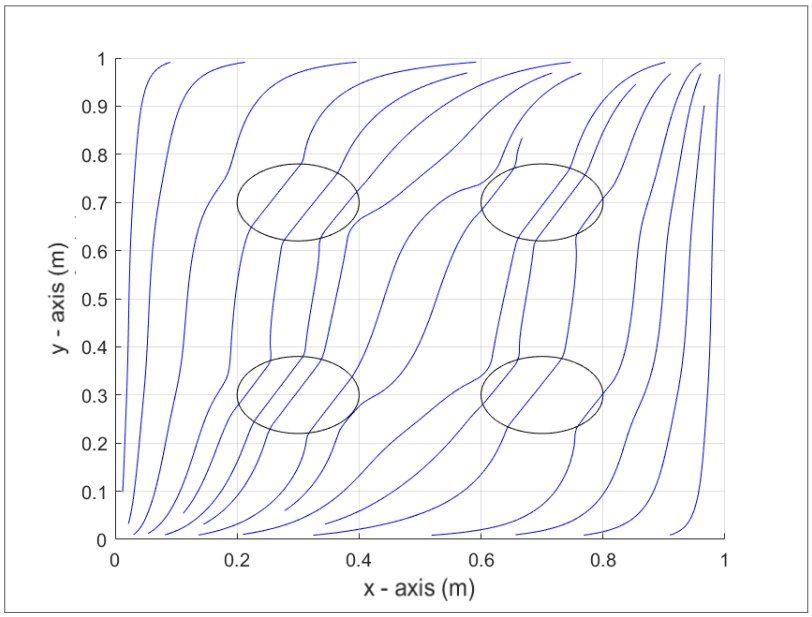

Source: Author.

5.4 ONE PHASE FLOW IN A POROUS DOMAIN WITH DISTRIBUTED VUGGY STRUCTURES CONNECTED BY A NETWORK OF FRACTURES WITH A 1/4 OF FIVE-SPOT CONFIGURATION

In the last case, inspired from one of the cases presented in (HE et al., 2015), we consider a carbonate rock with twenty five vugs distributed throughout the domain with a network of fourteen fractures connecting some of these vugs. The domain is a square defined by $[100mx100m]$. The permeability is given by $\mathbf{K} = k\mathbf{I}$ with $k = 1.5 \times 10^{-}15\, m^2$ for the porous media region and $k = 1.5 \times 10^{-}12\, m^2$ for the vugs and the fractures. The prescribed pressure on the injection well, which is placed in the bottom left part of the reservoir is given by $p_i = 3.13 \times 10^7 Pa$ and the prescribed pressure on the producer well, located in the right upper part of the reservoir is given by $p_p = 2.95 \times 10^7 Pa$ (see Figure 28). Null flux boundary conditions are set for all external faces of the domain. For this problem we have decided to use the unstructured triangular mesh with 61,952 control volumes.

Figure 28 – One Phase Flow in a Porous Domain with Distributed Vuggy Structures Connected by a Network of Fractures with a 1/4 of Five-spot Configuration: Geometry and model description for the 1/4 of five-spot configuration in a reservoir with vugy structures connected by a network of fractures.

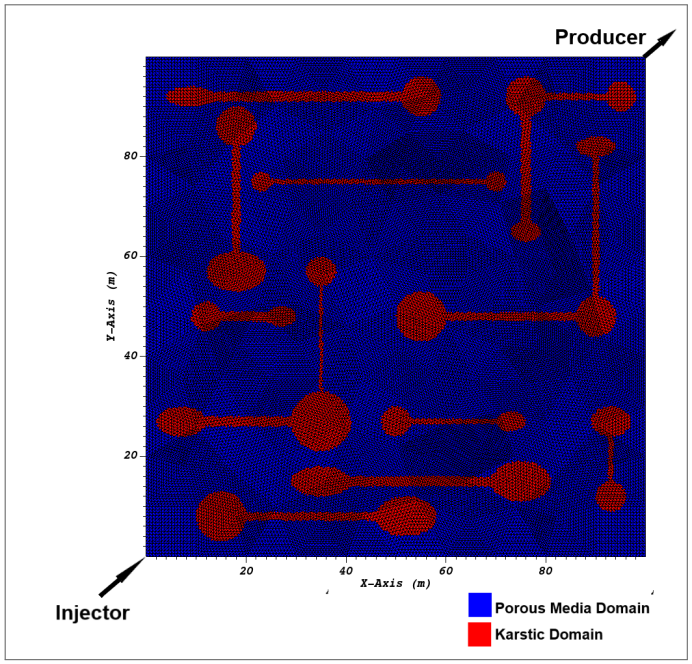

Source: Author.

Figure 29 – One Phase Flow in a Porous Domain with Distributed Vuggy Structures Connected by a Network of Fractures with a 1/4 of Five-spot Configuration: Pressure contours for the 1/4 of five-spot configuration in a reservoir with vuggy structures connected by a network of fractures with an unstructured triangular mesh with 61,952 control volumes.

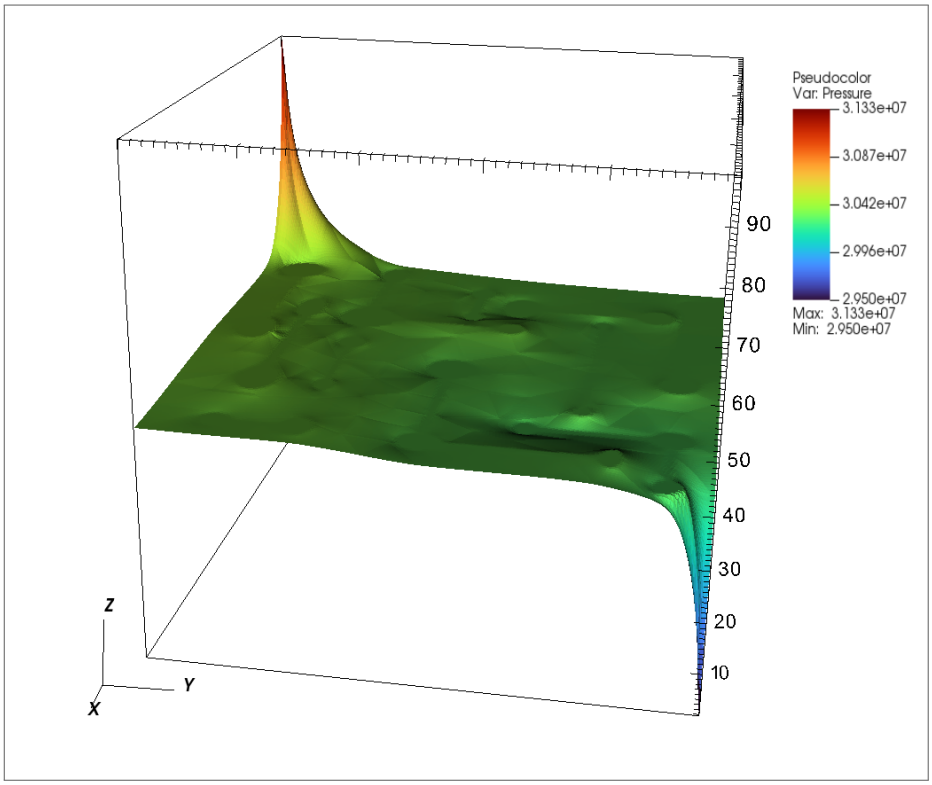

Source: Author.

In Figure 29, as it can be clearly seen, it is evident the strong influence of the vuggy and fracture structures in the pressure field and, consequently, in the fluid flow throughout the carbonate reservoir rock. It is wroth mentioning that our results compare quite well with those presented in (HE et al., 2015).

6 CONCLUSIONS AND FURTHER WORK

In this work, we presented and implemented a full pressure support Multipoint Flux Approximation method based on harmonic points (MPFA-H) for the numerical simulation of the one-phase flow in carbonate petroleum reservoirs using unstructured meshes. In that fashion, we analysed the influence of the karstic structures on the fluid flow. In order to solve the Stokes Brinkman's equation with the proposed scheme, two approaches were adopted: monolithic, in which the conservation of momentum equation and the mass conservation equation are solved simultaneously, and the segregated approach, in which the the conservation of momentum equation and the mass conservation equation are solved apart.

In the Stokes-Brinkman model, a single equation is used to model the fluid flow on the porous media and free flow regions. Furthermore, by adopting this approach, there is no need of modeling, explicitly, interface conditions alongside the different flow regions

It is important to highlight the contributions of the present work, in which, for the first time in literature, the MPFA-H method was extended to discretize the Stokes Brinkman's equations. Moreover, in order to guarantee the proper coupling between the pressure and velocity variables, avoiding the odd-even decoupling and oscilations of the pressure field, a modification of Rhie-Chow's interpolation method (ZHANG; ZHAO; BAYYUK, 2014). In order to verify the proposed formulation, we solved some benchmarks found in literature for one-phase flow problems, using unstructured meshes.

For all cases, the results obtained with our formulation were similar to the adopted references, representing in a coherent form the fluid flow on the porous domain, in which the flow is essentially Darcian, and in the free flow region. Finally, we verify the importance to adopt appropriate methods to properly represent the vuggy regions, once the presence of these structures alter significantly the fluid flow on these reservoirs.

Ultimately, some suggestions for future work:

- Extend the proposed formulation for three-dimensional domains and two-phase flows;
- Implement multiscale methods to solve the Stokes-Brinkman's equation;
- Implement numerical upscaling methods for modeling the fluid flow on carbonate petroleum reservoirs;
- Improve the physical model to include gravity and capillarity effects.

REFERENCES

AAVATSMARK, I.; BARKVE, T.; BØE, O.; MANNSETH, T. Discretization on unstructured grids for inhomogeneous, anisotropic media. part i: Derivation of the methods. *SIAM Journal on Scientific Computing*, SIAM, v. 19, n. 5, p. 1700–1716, 1998.

AAVATSMARK, I.; BARKVE, T.; BØE, O.; MANNSETH, T. Discretization on unstructured grids for inhomogeneous, anisotropic media. part ii: Discussion and numerical results. *SIAM Journal on Scientific Computing*, SIAM, v. 19, n. 5, p. 1717–1736, 1998.

AGELAS, L.; EYMARD, R.; HERBIN, R. A nine-point finite volume scheme for the simulation of diffusion in heterogeneous media. *Comptes Rendus Mathematique*, v. 347, n. 11, p. 673 – 676, 2009. ISSN 1631-073X.

AGUERRE, H. J.; VENIER, C. M.; PAIRETTI, C. I.; DAMIÁN, S. M.; NIGRO, N. M. A simple-based algorithm with enhanced velocity corrections: The complex method. *Computers Fluids*, v. 198, p. 104396, 2020. ISSN 0045-7930. Available at: <https://www.sciencedirect.com/science/article/pii/S0045793019303548>.

AHMED, R.; EDWARDS, M.; LAMINE, S.; HUISMAN, B.; PAL, M. Control-volume distributed multi-point flux approximation coupled with a lower-dimensional fracture model. *Journal of Computational Physics*, v. 284, p. 462–489, 2015. ISSN 0021-9991. Available at: <https://www.sciencedirect.com/science/article/pii/S0021999114008705>.

AHR, W. M.; ALLEN, D.; BOYD, A.; BACHMAN, H. N.; SMITHSON, T.; CLERKE, E.; GZARA, K.; HASSALL, J.; MURTY, C.; ZUBARI, H. et al. Confronting the carbonate conundrum. *Oilfield Review*, v. 17, n. 1, p. 18–29, 2005.

ARBOGAST, T.; LEHR, H. L. Homogenization of a darcy–stokes system modeling vuggy porous media. *Computational Geosciences*, Springer Science and Business Media LLC, v. 10, n. 3, p. 291–302, jul 2006. Available at: <https://doi.org/10.10072Fs10596-006-9024-8>.

AURIAULT, J.-L.; BOUTIN, C.; GEINDREAU, C. *Homogenization of coupled phenomena in heterogenous media*. [S.l.]: John Wiley & Sons, 2010.

BATCHELOR, G. K. *An Introduction to Fluid Dynamics*. Cambridge University Press, 2000. Available at: <https://doi.org/10.1017%2Fcbo9780511800955>.

BEAR, J. *Dynamics of fluids in porous media*. [S.l.]: Courier Corporation, 2013.

BI, L.; QIN, G.; POPOV, P.; EFENDIEV, Y.; ESPEDAL, M. An efficient upscaling process based on a unified fine-scale multi-physics model for flow simulation in naturally fracture carbonate karst reservoirs. In: *SPE/EAGE Reservoir Characterization and Simulation Conference*. Society of Petroleum Engineers, 2009. Available at: <https://doi.org/10.21182F125593-ms>.

BRINKMAN, H. C. A calculation of the viscous force exerted by a flowing fluid on a dense swarm of particles. *Flow, Turbulence and Combustion*, Springer Science and Business Media LLC, v. 1, n. 1, dec 1949.

CARMAN, P. C. Fluid flow through granular beds. *Chemical Engineering Research and Design*, Elsevier, v. 75, p. S32–S48, 1997.

CARVALHO, D. K. E. *Uma Formulação do Método dos Volumes Finitos com Estrutura de Dados por Aresta para a Simulação de Escoamento em Meio Poroso*. Phd Thesis (PhD Thesis) — Federal University of Pernambuco, 2005.

CARVALHO, D. K. E. D.; WILLMERSDORF, R. B.; LYRA, P. R. M. Some results on the accuracy of an edge-based finite volume formulation for the solution of elliptic problems in non-homogeneous and non-isotropic media. *International journal for numerical methods in fluids*, Wiley Online Library, v. 61, n. 3, p. 237–254, 2009.

CAVALCANTE, T. d. M.; CONTRERAS, F. R. L.; LYRA, P. R.; CARVALHO, D. K. E. de. A multipoint flux approximation with diamond stencil finite volume scheme for the two-dimensional simulation of fluid flows in naturally fractured reservoirs using a hybrid-grid method. *International Journal for Numerical Methods in Fluids*, Wiley Online Library, v. 92, n. 10, p. 1322–1351, 2020.

CHORIN, A. J. Numerical solution of the navier-stokes equations. *Mathematics of computation*, v. 22, n. 104, p. 745–762, 1968.

CHORIN, A. J. A numerical method for solving incompressible viscous flow problems. *Journal of computational physics*, Elsevier, v. 135, n. 2, p. 118–125, 1997.

ČIEGIS, R.; ILIEV, O.; LAKDAWALA, Z. On parallel numerical algorithms for simulating industrial filtration problems. *Computational Methods in Applied Mathematics*, De Gruyter, v. 7, n. 2, p. 118–134, 2007.

CONCEIÇÃO, S. B.; SEIDEL, M. A.; LYRA, P. R. M.; CARVALHO, D. K. E. de. Numerical simulation of flows in carbonate reservoirs using a stokes-brinkman model and locally conservative methods. In: 25^{th} ABCM INTERNATIONAL CONGRESS OF MECHANICAL ENGINEERING ,UBERLÂNDIA, MG, BRAZIL. *Proceedings of the COBEM*. [S.l.], 2019.

CONTRERAS, F.; LYRA, P. R.; SOUZA, M.; CARVALHO, D. K. E. de. A cell-centered multipoint flux approximation method with a diamond stencil coupled with a higher order finite volume method for the simulation of oil–water displacements in heterogeneous and anisotropic petroleum reservoirs. *Computers & Fluids*, Elsevier, v. 127, p. 1–16, 2016.

CONTRERAS, F. R.; LYRA, P. R.; de Carvalho, D. K. A new multipoint flux approximation method with a quasi-local stencil (mpfa-ql) for the simulation of diffusion problems in anisotropic and heterogeneous media. *Applied Mathematical Modelling*, v. 70, p. 659–676, 2019. ISSN 0307-904X. Available at: <https://www.sciencedirect.com/science/article/pii/S0307904X19300629>.

CONTRERAS, F. R. L. A MPFA Method Using Harmonic Points coupled to a Multidimensional Optimal Order Detection Method (mood) for the Simulation of Oil-Water Displacements in Petroleum Reservoirs. In: XXXVII IBERIAN LATIN AMERICAN CONGRESS ON COMPUTATIONAL METHODS IN ENGINEERING. *Revista Interdisciplinar De Pesquisa Em Engenharia*. Brasília,Brazil, 2016. p. 76–95.

CONTRERAS, F. R. L.; SOUZA, M. R. A.; LYRA, P. R. M.; CARVALHO, D. K. E. A mpfa method using harmonic points coupled to a multidimensional optimal order detection method (mood) for the simulation of oil-water displacements in petroleum reservoirs. *Revista Interdisciplinar de Pesquisa em Engenharia*, v. 2, n. 21, p. 76–95, 2017.

DABBOUK, C.; LIAQAT, A.; WILLIAMS, G.; BEATTIE, G. Waterflood in vuggy layer of a middle east reservoir - displacement physics understood. In: *Abu Dhabi International Petroleum Exhibition and Conference*. Society of Petroleum Engineers, 2002. Available at: <https://doi.org/10.21182F78530-ms>.

DARCY, H. Les fontaines publiques de la ville de dijon (the public fountains of the city of dijon). *Dalmont, Paris*, 1856.

DOORMAAL, J. P. V.; RAITHBY, G. D. Enhancements of the simple method for predicting incompressible fluid flows. *Numerical heat transfer*, Taylor & Francis, v. 7, n. 2, p. 147–163, 1984.

DOROBEK, S.; PICCOLI, L.; COFFEY, B.; ADAMS, A. Carbonate rock-forming processes in the pre-salt "sag" successions of campos basin, offshore brazil: evidence for seasonal, dominantly abiotic carbonate precipitation, substrate controls, and broader geologic implications. In: *AAPG Hedberg Conference "Microbial Carbonate Reservoir Characterization" Houston Texas*. [S.l.: s.n.], 2012.

DREW, D. A.; PASSMAN, S. L. *Theory of Multicomponent Fluids*. [S.l.]: Springer New York, 1999.

EWING, R. E. *The Mathematics of Reservoir Simulation*. Society for Industrial and Applied Mathematics, 1983. Available at: <https://epubs.siam.org/doi/abs/10.1137/1.9781611971071>.

FERZIGER, J. H.; PERIĆ, M.; STREET, R. L. *Computational Methods for Fluid Dynamics*. [S.l.]: Springer International Publishing, 2020.

FRIIS, H. A.; EDWARDS, M. G. A family of mpfa finite-volume schemes with full pressure support for the general tensor pressure equation on cell-centered triangular grids. *Journal of Computational Physics*, v. 230, n. 1, p. 205–231, 2011. ISSN 0021-9991. Available at: <https://www.sciencedirect.com/science/article/pii/S0021999110005061>.

FUHRMANN, J.; OHLBERGER, M.; ROHDE, C. *Finite Volumes for Complex Applications VII: Methods and Theoretical Aspects*. [S.l.]: Springer International Publishing, 2014.

GAO, Z.; WU, J. A small stencil and extremum-preserving scheme for anisotropic diffusion problems on arbitrary 2d and 3d meshes. *J. Comput. Phys.*, v. 250, p. 308–331, 2013.

GAO, Z.-M.; WU, J.-M. A linearity-preserving cell-centered scheme for the anisotropic diffusion equations. In: *Finite Volumes for Complex Applications VII-Methods and Theoretical Aspects*. Springer International Publishing, 2014. p. 293–301. Available at: <https://doi.org/10.10072F978-3-319-05684-5_28>.

GLOVER, C. *Conservation principles of continuous media /*. 3rd ed.. ed. [S.l.]: McGraw-Hill,, 1994. ISBN 0070240396.

GOLFIER, F.; LASSEUX, D.; QUINTARD, M. Investigation of the effective permeability of vuggy or fractured porous media from a darcy-brinkman approach. *Computational Geosciences*, Springer Science and Business Media LLC, v. 19, n. 1, p. 63–78, oct 2014. Available at: <https://doi.org/10.10072Fs10596-014-9448-5>.

HALLACK, D. M. C.; FILHO, J. S. D. A. C.; COUTO, P. Implementation of a two-phase simulator based on the brinkman's equation for vuggy-karstified reservoirs. In: *Offshore Technology Conference Brasil*. [S.l.]: Offshore Technology Conference, 2019.

HARTEN, A. The artificial compression method for computation of shocks and contact discontinuities. iii. self-adjusting hybrid schemes. *Mathematics of Computation*, v. 32, n. 142, p. 363–389, 1978.

HE, J.; KILLOUGH, J. E.; F., M. M. F.; FRAIM, M. A unified finite difference model for the simulation of transient flow in naturally fractured carbonate karst reservoirs. In: *SPE Reservoir Simulation Symposium*. [S.l.]: Society of Petroleum Engineers, 2015.

HIRSCH, C. Numerical computation of internal and external flows (vol1: Fundamentals of numerical discretization). In: . [S.l.: s.n.], 2007.

HONÓRIO, H. T. *Análise de Métodos Segregados e Acoplado de Solução de Escoamentos Incompressíveis Utilizando Malhas Não-Estruturadas Híbridas*. Phd Thesis (PhD Thesis) — UNIVERSIDADE FEDERAL DE SANTA CATARINA, Florianópolis - Brazil, 2013.

ILIEV, O.; KIRSCH, R.; LAKDAWALA, Z.; PRINTSYPAR, G. Mpfa algorithm for solving stokes-brinkman equations on quadrilateral grids. In: *Finite Volumes for Complex Applications VII-Elliptic, Parabolic and Hyperbolic Problems*. [S.l.]: Springer, 2014. p. 647–654.

JHA, B. K.; KAURANGINI, M. L. Approximate analytical solutions for the nonlinear brinkman-forchheimer-extended darcy flow model. *Applied Mathematics*, Scientific Research Publishing, Inc„ v. 02, n. 12, p. 1432–1436, 2011.

KIM, J.; MOIN, P. Application of a fractional-step method to incompressible navier-stokes equations. *Journal of computational physics*, Elsevier, v. 59, n. 2, p. 308–323, 1985.

KROTKIEWSKI, M.; LIGAARDEN, I. S.; LIE, K.-A.; SCHMID, D. W. On the importance of the stokes-brinkman equations for computing effective permeability in karst reservoirs. *Communications in Computational Physics*, Global Science Press, v. 10, n. 5, p. 1315–1332, nov 2011.

LAPTEV, V. *Numerical solution of coupled flow in plain and porous media*. Phd Thesis (doctoralthesis) — Technische Universität Kaiserslautern, 2003. Available at: <http://nbn-resolving.de/urn:nbn:de:hbz:386-kluedo-17312>.

LIPNIKOV, K.; SHASHKOV, M.; SVYATSKIY, D.; VASSILEVSKI, Y. Monotone finite volume schemes for diffusion equations on unstructured triangular and shape-regular polygonal meshes. *Journal of Computational Physics*, Elsevier BV, v. 227, n. 1, p. 492–512, nov 2007. Available at: <https://doi.org/10.10162Fj.jcp.2007.08.008>.

MAJUMDAR, S. Role of Underrelaxation in Momentum Interpolation for Calculation of Flow With Nonstaggered Grids. *Numerical Heat Transfer*, Informa UK Limited, v. 13, n. 1, p. 125–132, jan 1988.

MARCHI, C. H.; MALISKA, C. R. A Nonorthogonal Finite-Volume Method For The Solution Of All Speed Flows Using Co-Located Variables. *Numerical Heat Transfer, Part B: Fundamentals*, Informa UK Limited, v. 26, n. 3, p. 293–311, oct 1994.

MARTYS, N.; BENTZ, D. P.; GARBOCZI, E. J. Computer simulation study of the effective viscosity in brinkman's equation. *Physics of Fluids*, American Institute of Physics, v. 6, n. 4, p. 1434–1439, 1994.

MAZHAR, Z. An enhancement to the block implicit procedure for the treatment of the velocity-pressure coupling problem in incompressible fluid flow. *Numerical Heat Transfer: Part B: Fundamentals*, Taylor & Francis, v. 41, n. 5, p. 493–500, 2002.

MAZUMDER, S. *Numerical methods for partial differential equations: finite difference and finite volume methods*. [S.l.]: Academic Press, 2015.

OLSON, J. E.; LAUBACH, S. E.; LANDER, R. H. Combining diagenesis and mechanics to quantify fracture aperture distributions and fracture pattern permeability. *Geological Society, London, Special Publications*, Geological Society of London, v. 270, n. 1, p. 101–116, 2007.

PATANKAR, S. V. *Numerical Heat Transfer and Fluid Flow*. [S.l.]: CRC Press, 2018.

PATANKAR, S. V.; SPALDING, D. B. A calculation procedure for heat, mass and momentum transfer in three-dimensional parabolic flows. In: *Numerical prediction of flow, heat transfer, turbulence and combustion*. [S.l.]: Elsevier, 1983. p. 54–73.

POTIER, C. L. A nonlinear finite volume scheme satisfying maximum and minimum principles for diffusion operators. *International Journal on Finite Volumes*, Institut de Mathématiques de Marseille, AMU, p. 1–20, Dec. 2009. Available at: <https://hal.archives-ouvertes.fr/hal-01116968>.

QUEIROZ, L.; SOUZA, M.; CONTRERAS, F.; LYRA, P. R. M.; CARVALHO, D. K. E. de. On the accuracy of a nonlinear finite volume method for the solution of diffusion problems using different interpolations strategies. *International Journal for Numerical Methods in Fluids*, Wiley Online Library, v. 74, n. 4, p. 270–291, 2014.

RHIE, C. M.; CHOW, W. L. Numerical study of the turbulent flow past an airfoil with trailing edge separation. *AIAA Journal*, American Institute of Aeronautics and Astronautics (AIAA), v. 21, n. 11, p. 1525–1532, nov 1983.

SCHNEIDER, G. E.; RAW, M. J. Control Volume Finite-Element Method for Heat Transfer and Fluid Flow Using Collocated Variables— 1. Computational Procedure. *Numerical Heat Transfer*, Informa UK Limited, v. 11, n. 4, p. 363–390, apr 1987.

SPADINI, A. et al. Carbonate reservoirs in brazilian sedimentary basins. In: WORLD PETROLEUM CONGRESS. *19th World Petroleum Congress*. [S.l.], 2008.

STOKES, G. III. on the aberration of light. *The London, Edinburgh, and Dublin Philosophical Magazine and Journal of Science*, Informa UK Limited, v. 27, n. 177, p. 9–15, jul 1845.

TEIXEIRA, J. C.; GUIMARÃES, L. J. do N.; CARVALHO, D. K. E. Streamline-based simulation in highly heterogeneous and anisotropic petroleum reservoirs using a non-orthodox mpfa method and an adaptive timestep strategy with unstructured meshes. *Journal of Petroleum Science and Engineering*, Elsevier, p. 108369, 2021.

TEMAM, R. Une méthode d'approximation de la solution des équations de navier-stokes. *Bulletin de la Société Mathématique de France*, v. 96, p. 115–152, 1968.

VELAZQUEZ, R. C.; VASQUEZ-CRUZ, M. A.; CASTREJON-AIVAR, R.; ARANA-ORTIZ, V. Pressure transient and decline curve behaviors in naturally fractured vuggy carbonate reservoirs. *SPE Reservoir Evaluation & Engineering*, Society of Petroleum Engineers (SPE), v. 8, n. 02, p. 95–112, apr 2005. Available at: <https://doi.org/10.21182F77689-pa>.

WANG, H.; WANG, H.; GAO, F.; ZHOU, P.; ZHAI, Z. J. Literature review on pressure–velocity decoupling algorithms applied to built-environment cfd simulation. *Building and Environment*, Elsevier, v. 143, p. 671–678, 2018.

WU, Y.-S.; EHLIG-ECONOMIDES, C. A.; QIN, G.; KANG, Z.; ZHANG, W.; AJAYI, B. T.; TAO, Q. A triple-continuum pressure-transient model for a naturally fractured vuggy reservoir. In: *SPE Annual Technical Conference and Exhibition*. Society of Petroleum Engineers, 2007. Available at: <https://doi.org/10.21182F110044-ms>.

YAO, J.; HUANG, Z.; LI, Y.; WANG, C.; LV, X. Discrete fracture-vug network model for modeling fluid flow in fractured vuggy porous media. In: *International Oil and Gas Conference and Exhibition in China*. Society of Petroleum Engineers, 2010. Available at: <https://doi.org/10.21182F130287-ms>.

YUAN, G.; SHENG, Z. Monotone finite volume schemes for diffusion equations on polygonal meshes. *Journal of Computational Physics*, v. 227, n. 12, p. 6288 – 6312, 2008. ISSN 0021-9991.

ZHANG, S.; ZHAO, X.; BAYYUK, S. Generalized formulations for the rhie–chow interpolation. *Journal of Computational Physics*, v. 258, p. 880–914, 2014.

APPENDIX A – RESUMO ESTENDIDO

UM MÉTODO DE APROXIMAÇÃO DE FLUXO POR MÚLTIPLOS PONTOS PARA A SIMULAÇÃO NUMÉRICA DO MODELO DE STOKES-BRINKMAN EM 2-D UTILIZANDO MALHAS NÃO ESTRUTURADAS

Introdução

Reservatórios carbonáticos são comumente encontrados em todo mundo, como por exmplo na China (AHR et al., 2005), Oriente Médio (DABBOUK et al., 2002) e na região do Pré-Sal brasileiro (DOROBEK et al., 2012). Estima-se que, cerca de 60% das reservas mundiais de petróleo estão nos reservatórios carbonáticos (SPADINI et al., 2008).

Devido aos processos diagenéticos que ocorrem nestes reservatórios, aliado a natureza química das rochas carbonáticas e aos fenômenos de tectonização e casrtificação, originam estruturas geológicas como *vugs*, vazios pequenos e médios, e cavernas, que podem ou não estar interconectados, envolvendo mútliplas escalas (BI et al., 2009; KROTKIEWSKI et al., 2011; HE et al., 2015).

A presença destas estruturas geológicas em múltiplas escalas, representa um desafio para a simulação do escoamento nestes reservatórios devido à grande heterogeneidade nas propriedades da rocha e à coexistência de duas regiões de escoamento distintas, uma região de escoamento em meio poroso, Darciniana, e uma região de escoamento livre, na região dos *vugs* e cavernas, tornando o modelo numérico aproximado para o escoamento de fluidos desafiador (CONCEIÇÃO et al., 2019). Diferentes modelos são utilizados para representar o escoamento nestes reservatórios como os modelos de dupla ou tripla porosidade, tripla permeabilidade e o modelo Darcy-Stokes (VELAZQUEZ et al., 2005; WU et al., 2007; YAO et al., 2010; HALLACK; FILHO; COUTO, 2019).

Uma vez que reservatórios carbonáticos são muito heterogêneos, a utilizaçao destes modelos pode representar um grande custo computacional e complexidade ao modelo devido à necessidade de condições de interface (CONCEIÇÃO et al., 2019). Uma abordagem alternativa é a utilziação do modelo de Stokes Brinkman (BRINKMAN, 1949), onde uma única equação é capaz de representar o escoamento de fluido nas duas regiões, meio poroso e escoamento livre.

Métodos de aproximação de fluxo por múltiplos pontos (MPFA) tem sido largamente utilizados em problemas de escoamento em meio poroso (CAVALCANTE et al., 2020; CONTRERAS et al., 2016). Métodos MPFA são robustos e flexíveis para lidar com tensores de permeabilidade cheios e malhas poligonais quaisquer. Nesta dissertação, um método MPFA com suporte completo de pressão, originalmente proposto por Gao and Wu (2013), é extendido para discretizar a Equação de Stokes-Brinkman em reservatórios carbonáticos.

Objetivos Gerais

O objetivo geral do presente trabalho é o estudo e desenvolvimento de um método de volumes finitos em 2-D para a simulação numérica do escoamento monofásico em reservatórios carbonáticos heterogêneos e anisotrópicos, utilizando malhas poligonais quaisquer.

Objetivos Específicos

1. Desenvolver um *framework* para a simulação do escoamento monofásico em reservatórios carbonáticos heterogêneos e anisotrópicos consistente com malhas não estruturadas.

2. Incorporar o MPFA-H para solução da Equação de Stokes-Brinkman.

3. Investigar a influência das estruturas cársticas nos campos de pressão e velocidade, considerando um escoamento incompressível.

Formulação Matemática

Devido à complexidade associada ao escoamento nestes reservatórios, neste trabalho algumas hipóteses simplificadoras foram feitas como: o escoamento é considerado monofásico, o fluido é Newtoniano, a rocha é incompressível e está totalmente saturada com fluido, efeitos térmicos, uímicos e gravidade são desconsiderados.

Equação de Stokes-Brinkman

A Equação de Stokes-Brinkman, considerando um escoamento incompressível no regime transiente é dada por:

$$\frac{\partial(\rho \mathbf{u})}{\partial t} + \mu \mathbf{K}^{-1}\mathbf{u} - \mu^{'}\nabla^2\mathbf{u} = -\nabla p \tag{A.1}$$

onde $\mathbf{u}$ é o vetor velocidade, p representa a pressão do fluido, ρ é a densidade do fluido, μ a viscosidade dinâmica e $\mathbf{K}$ é o tensor de permeabilidade absoluto da rocha.

Equação de Conservação da Massa

Considerando o fluido incompressível e homogêneo, ou seja, a densidade não varia no tempo e no espaço, e na ausência de termos fonte ou sumidouro, a equação de conservação da massa é dada por (FERZIGER; PERIĆ; STREET, 2020):

$$\nabla \cdot \mathbf{u} = 0 \tag{A.2}$$

Condições Iniciais e de Contorno

Para tornar o modelo matemático descrito acima bem-posto, devemos propor condições de contorno e condições iniciais consistentes. As condições de contorno usuais para o problema são (CARVALHO, 2005; CONTRERAS et al., 2017; CONCEIÇÃO et al., 2019):

$$\begin{aligned} p(\mathbf{x_D}, t) &= g_D \quad \text{in} \quad \Gamma_D \times T \\ \mathbf{u} \cdot \mathbf{n} &= g_N \quad \text{in} \quad \Gamma_N \times T \\ \mathbf{u}(\mathbf{x}, 0) &= \mathbf{u}^0 \quad \text{in} \quad \Omega \quad at \quad t = 0 \\ \mathbf{u}(\mathbf{x}, t) &= 0 \quad in \quad \Gamma_S \times T \end{aligned} \tag{A.3}$$

onde Γ_D e Γ_N representam as fronteiras do contorno de Dirichlet e Neumann, respectivamente, Γ_S são as paredes sólidas e T é o intervalo da análise. O escalar g_D (pressão prescrita) e g_N (fluxo prescrito) são aplicadoes em Γ_D e Γ_N, respectivamente.

Formulação Numérica

As equações de conservação do momento linear e de conservação da massa são então discretizadas utilizando um esquema da família dos volumes finitos. Além disso, para garantir o acoplamneto entre as variáveis, pressão e velocidade, foi utilizado um método de interpolação do momento (ZHANG; ZHAO; BAYYUK, 2014), o qual consiste em uma modificação do Método de Rhie-Chow (RHIE; CHOW, 1983).

Gradiente de Pressão

Para estimar o gradiente de pressão em cada volume de controle Ω_v, é

necessário estimar o valor da pressão nos chamados pontos harmônicos.

$$-\sum_{i=1}^{n_v}\int_{\Omega_{\hat{L}}}\nabla p\, d\Omega_{\hat{L}} = -\sum_{IJ\in\Gamma_{\hat{L}}}\int_{IJ} p\mathbf{n}_{\Gamma_{IJ}} ds = -\sum_{IJ\in\Gamma_{\hat{L}}} p_{IJ}\,\|IJ\|\,\mathbf{n}_{IJ} \tag{A.4}$$

onde p_{IJ} é a pressão nos pontos harmônicos, IJ é área da face (comprimento em 2-D) e $\mathbf{n_{IJ}}$ é o vetor normal unitário associado à face.

A definição e derivação dos pontos harmônicos neste trabalho segue aquele definido por Agelas, Eymard and Herbin (2009).

Considerando dois volumes de controle, $\hat{L}$ e $\hat{R}$, adjacentes a uma face IJ do domínio, com tensores de permeablidade $\mathbf{K_{\hat{L}}}$ e $\mathbf{K_{\hat{R}}}$, respectivamente, cujos centróides são designados por $x_{\hat{L}}$ e $x_{\hat{R}}$. Desta forma, o ponto de interpolação sobre a superfície IJ é definido por:

$$x_{\hat{L},i(IJ)} = \frac{h_{\widehat{L},IJ}k^{(n)}_{\widehat{R},IJ}x_{\widehat{R}} + h_{\widehat{R},IJ}k^{(n)}_{\widehat{L},IJ}x_{\widehat{L}} + h_{\widehat{L},IJ}h_{\widehat{R},IJ}\left(\mathbf{K}^{\top}_{\widehat{L}} - \mathbf{K}^{\top}_{\widehat{R}}\right)\mathbf{n}_{IJ}}{h_{\widehat{L},IJ}k^{(n)}_{\widehat{R},IJ} + h_{\widehat{R},IJ}k^{(n)}_{\widehat{L},IJ}} \tag{A.5}$$

Tendo definido o ponto harmônico, sabe-se que a pressão no mesmo é uma combinação convexa das pressões dos volumes de controle adjacentes (CONTRERAS et al., 2017). Desta forma a pressão na superfície de controle IJ é dada por:

$$p_{IJ} = \omega_{\hat{L},IJ}p_{\hat{L}} + \omega_{\hat{R},IJ}p_{\hat{R}} \tag{A.6}$$

onde os termos $\omega_{\hat{L},IJ}$ e $\omega_{\hat{R},IJ}$ são os pesos. Deve-se salientar que a interpolação da pressão nos pontos harmônicos preserva o princípio de linearidade (CONTRERAS et al., 2016).

$$\omega_{\hat{L},IJ} = \frac{h_{\hat{R},IJ}\,k^{(n)}_{\hat{L},IJ}}{h_{\hat{R},IJ}\,k^{(n)}_{\hat{L},IJ} + h_{\hat{L},IJ}\,k^{(n)}_{\hat{R},IJ}} \qquad \text{and} \qquad \omega_{\hat{R},IJ} = 1 - \omega_{\hat{L},IJ} \tag{A.7}$$

Termos Difusivos

Utilizamos um método com suporte completo de pressão para a aproximação dos fluxos das componentes da velocidade, u e v. Desta maneira, o fluxo único sob uma superfície de controle IJ é dado por:

$$\mathbf{F}_{\phi,IJ} \cdot \mathbf{N_{IJ}} = \sum_{\gamma=i,j} \sum_{\hat{r}=\hat{L},\hat{R}} \chi_{\hat{r},\gamma(IJ)}(\phi_{\hat{r}} - \phi_{\hat{r},\gamma(IJ)})\|\vec{IJ}\| \tag{A.8}$$

onde:

$\chi_{\hat{r},\gamma(IJ)} = w_{\hat{r},IJ}\xi_{\hat{r},\gamma(IJ)}$, com $\hat{r} = \hat{L}, \hat{R}$ e $\gamma = i, j$.

Finalmente, o valor das componentes da velocidade nos pontos harmônicos são definidas por: $\phi_{\hat{r},\gamma(IJ)} = \omega_{\hat{M},\gamma(IJ)}\phi_{\widehat{M},\gamma} + \omega_{\hat{N},\gamma(IJ)}\phi_{\widehat{N},\gamma}$, onde $\omega_{\hat{M},\gamma IJ} = \frac{h_{\widehat{M},\gamma(IJ)}}{h_{\widehat{M},\gamma(IJ)}+h_{\widehat{N},\gamma(IJ)}}$ and $\omega_{\hat{N},(IJ)} = 1 - \omega_{\hat{M},\gamma(IJ)}$, no qual M e N representam os volumes de controle adjacentes à face IJ.

Forma Final da Equação de Conservação do Momento

Após a discretização dos termos na equação de conservação do momento, considerando um volume de controle genérico $\hat{L}$ temos:

$$\frac{\rho V_{\hat{L}}}{\Delta t}\left({\phi_{\hat{L}}}^{n+1} - {\phi_{\hat{L}}}^{n}\right) + \mu V_{\hat{L}}\mathbf{K}^{-\mathbf{1}}_{\hat{\mathbf{L}}}\phi^{n+1}_{\hat{L}} + \sum_{\Gamma_{IJ}\in\Gamma_{\hat{L}}} \sum_{\gamma=i,j} \sum_{\hat{r}=\hat{L},\hat{R}} \|\vec{IJ}\|\chi_{\hat{r},\gamma(IJ)}(\phi_{\hat{r}} - \phi_{\hat{r},\gamma(IJ)})^{n+1}$$
$$= -\sum_{\Gamma_{IJ}\in\Gamma_{\hat{L}}} p^{n+1}_{IJ}\|IJ\|\mathbf{n}_{IJ} \tag{A.9}$$

Agrupando todos os termos relacionados às componentes de velocidade e ao gradiente de pressão, é possível reescrever a equação de conservação do momento de forma mais compacta, como:

$$a_{u,\hat{L}}u^{n+1}_{\hat{L}} = \sum_{i=1}^{nb}(a_{u,nb}u_{nb})^{n+1}_{P} - V_{\hat{L}}\left(\frac{\partial p}{\partial x}\right)^{n+1}_{\hat{L}} + \frac{\rho_{\hat{L}}V_{\hat{L}}}{\Delta t}u^{n}_{\hat{L}} \tag{A.10}$$

$$a_{v,\hat{L}}v^{n+1}_{\hat{L}} = \sum_{i=1}^{nb}(a_{v,nb}v_{nb})^{n+1}_{P} - V_{\hat{L}}\left(\frac{\partial p}{\partial y}\right)^{n+1}_{\hat{L}} + \frac{\rho_{\hat{L}}V_{\hat{L}}}{\Delta t}v^{n}_{\hat{L}} \tag{A.11}$$

Interpolação das Velocidades nas Faces

Com o objetivo de garantir o acoplamento entre as variáveis, pressão e velocidade, foi utilizado uma estratégia de interpolação do momento (ZHANG; ZHAO; BAYYUK, 2014) para estimar as velocidades nas superfícies de controle IJ do domínio.

Desta forma, as velocidades nas faces IJ são dadas por:

$$u_{IJ} = \overline{u_{IJ}} + \frac{(1-\beta)V_{\hat{L}}}{a_{u,\hat{L}}}\left(\frac{\partial p}{\partial x}\right)_{\hat{L}}^{n+1} + \frac{\beta V_{\hat{R}}}{a_{u,\hat{R}}}\left(\frac{\partial p}{\partial x}\right)_{\hat{R}}^{n+1} - \frac{V_{IJ}}{a_{u,IJ}}\left(\frac{\partial p}{\partial x}\right)_{IJ}^{n+1} + \frac{\rho_{IJ}V_{IJ}}{a_{u,IJ}\,\Delta t}u_{IJ}^{n} \tag{A.12}$$

onde

$$u_{IJ}^{n} = \left[\frac{(1-\beta)V_{\hat{L}}}{a_{u,\hat{L}}}\left(\frac{\partial p}{\partial x}\right)_{\hat{L}} + \frac{\beta V_{\hat{R}}}{a_{u,\hat{R}}}\left(\frac{\partial p}{\partial x}\right)_{\hat{R}} - \frac{V_{IJ}}{a_{u,IJ}}\left(\frac{\partial p}{\partial x}\right)_{IJ}\right]^{n} \tag{A.13}$$

De maneira similar, podemos escrever a velocidade na face para a componente v como:

$$v_{IJ} = \overline{v_{IJ}} + \frac{(1-\beta)V_{\hat{L}}}{a_{u,\hat{L}}}\left(\frac{\partial p}{\partial y}\right)_{\hat{L}}^{n+1} + \frac{\beta V_{\hat{R}}}{a_{v,\hat{R}}}\left(\frac{\partial p}{\partial y}\right)_{\hat{R}}^{n+1} - \frac{V_{IJ}}{a_{v,IJ}}\left(\frac{\partial p}{\partial y}\right)_{IJ}^{n+1} + \frac{\rho_{IJ}V_{IJ}}{a_{v,IJ}\,\Delta t}v_{IJ}^{n} \tag{A.14}$$

onde

$$v_{IJ}^{n} = \left[\frac{(1-\beta)V_{\hat{L}}}{a_{v,\hat{L}}}\left(\frac{\partial p}{\partial y}\right)_{\hat{L}} + \frac{\beta V_{\hat{R}}}{a_{v,\hat{R}}}\left(\frac{\partial p}{\partial y}\right)_{\hat{R}} - \frac{V_{IJ}}{a_{v,IJ}}\left(\frac{\partial p}{\partial y}\right)_{IJ}\right]^{n} \tag{A.15}$$

Ao assumirmos esta aproximação para o termo transiente, este tende a estabilzar o método à medida que o passo de tempo diminui.

Conclusão

Neste trabalho, apresentamos e implementamos um método de Aproximação de Fluxo por Múltiplos Pontos com suporte de pressão completo baseado em pontos harmônicos (MPFA-H) para a simulação numérica do escoamento

monofásico em reservatórios de petróleo carbonáticos usando malhas não-estruturadas. Dessa forma, analisamos a influência das estruturas cársticas no escoamento do fluido. Para resolver a equação de Stokes Brinkman com o esquema proposto, duas abordagens foram adotadas: a monolítica, em que a equação de conservação da quantidade de movimento e a equação de conservação de massa são resolvidas simultaneamente, e a abordagem segregada, na qual a equação de conservação de quantidade de movimento e as equações de conservação de massa são resolvidas separadamente.

É importante destacar as contribuições do presente trabalho, no qual, pela primeira vez na literatura, o método MPFA-H foi estendido para discretizar as equações de Stokes Brinkman. Além disso, a fim de garantir o acoplamento adequado entre as variáveis de pressão e velocidade, evitando o desacoplamento par-ímpar e oscilações do campo de pressão, foi utilzado uma modificação do método de interpolação de Rhie-Chow (ZHANG; ZHAO; BAYYUK, 2014). Para verificar a formulação proposta, resolvemos alguns benchmarks encontrados na literatura para problemas de escoamento monofásico, utilizando malhas não estruturadas.

Para todos os casos, os resultados obtidos com nossa formulação foram semelhantes às referências adotadas, representando de forma coerente o escoamento do fluido no domínio poroso, no qual o escoamento é essencialmente Darciniano, e na região de escoamento livre. Por fim, verificamos a importância da adoção de métodos adequados para representar adequadamente as regiões de vuggy, uma vez que a presença dessas estruturas altera significativamente o escoamento do fluido nesses reservatórios.